



# Synoptic characteristics of rainy winters over the northern Arabian Peninsula

Mana Ali Asiri<sup>1</sup> · Mansour Almazroui<sup>1</sup> · Abdulhaleem Hussin Labban<sup>1</sup> · Adel Mahmoud Awad<sup>1</sup> 

Received: 22 January 2021 / Accepted: 7 July 2021 / Published online: 31 July 2021  
© Saudi Society for Geosciences 2021

## Abstract

Surface observations of rain from 15 stations across the northern Arabian Peninsula (AP) and meteorological data from the NCEP/NCAR reanalysis data set were used to study the winter atmospheric factors and subtropical jet stream (STJ) characteristics controlling rain over the northern AP. The statistical study shows that January has the highest amount of winter rain when the STJ is at 200 hPa and is located in the zone between 25°N and 30°N. Synoptically, the northern AP winter rain forms when the Red Sea trough (RST) extends northward and is located to the east of the upper trough, while the rain decreases when the Siberian high intensifies, the pressure gradient around the RST decreases and the STJ becomes zonal or exits over the Middle East. Moreover, the study shows that the Mediterranean cyclone plays a secondary role in the generated rain, mainly producing atmospheric conditions favoring the northward extension of the RST. The results demonstrate that the pressure/geopotential gradient is more important than the relative positions of atmospheric systems in the development of rain. The temporal and vertical variations in the STJ indicate that the rain decreases as the core of the low-pressure difference shifts southward from the northern Red Sea. Additionally, the amount of the Siberian high difference is comparable to the negative low-pressure difference, while the Azores difference is relatively weak.

**Keywords** STJ variability · Winter rain · Arabian Peninsula · Atmospheric systems

## Introduction

The location of the Middle East and the Levant on the climatic border between temperate (Mediterranean) and arid climatic zones makes this region prone to droughts (Trewartha and Horn 1980; Alpert et al. 2002; Hasanean and Almazroui 2015), which are enhanced by dust storms (Parolari et al. 2016) and are influenced by mid-latitude and tropical atmospheric processes that play major roles during the rainy season (Krichak et al. 2000). Regional dry areas are sensitive not only to seasonal droughts but also to prolonged dry spells during the rainy season (Saaroni et al. 2019).

Rain events in semiarid and arid subtropical regions are characterized by a high rate of interannual variability (Lockwood 1988) and occur as a result of

tropical-extratropical interactions (Ziv 2001; Knippertz 2005; Ziv et al. 2005; De Vries et al. 2013; Martius et al. 2013). Furthermore, regional cyclogenesis and cyclone tracks influence the Mediterranean and produce favorable rainfall conditions (Alpert et al. 1990; Flocas and Giles 1991; Trigo et al. 1999; Maheras et al. 2001) that are strongly related to the prevailing circulation regime.

There are different explanations for the atmospheric systems that generate rain in the Middle East region. However, previous studies (Dayan and Sharon 1980; Dayan et al. 2001; Kahana et al. 2002) found that the annual rainfall in the arid region of the southern Levant was poorly correlated with both synoptic- and large-scale factors, i.e., the rain regime was dominated by local effects and convective systems. Ziv et al. (2014) found that annual rainfall may be controlled by large-scale oscillations both directly and indirectly via local systems. Generally, rain over the Levant region is produced not only by local mechanisms but also by large-scale oscillations, such as the North Atlantic Oscillation (NAO) and Arctic Oscillation (AO) (Eshel and Farrell 2000; Cullen et al. 2002; Dunkeloh and Jacobeit 2003; Raymond et al. 2018; Ghasemi and Khalili 2008; Oikonomou et al. 2010; Trambly and Hertig 2018; Saaroni et al. 2019), or negatively related to the

---

Responsible Editor: Zhihua Zhan

✉ Adel Mahmoud Awad  
awad\_adel@yahoo.com; amawad@kau.edu.sa

<sup>1</sup> Department of Meteorology, King Abdulaziz University, P.O. Box 80208, Jeddah 21589, Saudi Arabia

Azores high (Iqbal et al. 2013). Moreover, the central and eastern Mediterranean rain is mainly related to the Scandinavian pattern (Rogers 1990).

In their study on winter rain in the southern Levant, Kutiel and Paz (1998) found that at the beginning of the rainy season (October), rainfall is discontinuous and spotty without a distinctly coherent region, while at the end of the rainy season (April), rainfall is more widespread and forms a large coherent region.

With respect to rain formation, Ziv et al. (2006) indicated that rain is formed over the southern Levant within cold air masses of European origin that enter the region from the northwest and that through their movement over warmer Mediterranean waters, these masses gain moisture and become conditionally unstable. Seager et al. (2003) showed that an anomalously high sea surface temperature (SST) in the tropics enhances the Hadley circulation, including the subtropical jet stream (STJ) and the eastern Mediterranean trough, while Ben-Gai et al. (1994) indicated that a positive change in the SST increases rainfall over the Mediterranean region.

In detail, Dayan and Abramski (1983) attributed the heavy rains observed in February 1975 over the southern Levant to the abnormal shape of the STJ, which was tilted such that its axis at the 300 hPa level was abnormally positioned to the right (south) of its position at the 200 hPa level. In describing the relation between jets and rain, Niranjan Kumar et al. (2016) showed that the low-level convergence associated with the upper tropospheric divergence across the STJ should be considered a primary issue of winter convective activity over the AP. Moreover, the upper trough over the eastern Mediterranean (EM) induces cold advection aloft into the surface low-pressure system, which triggers and enhances tropical convection (Kiladis and Weickmann 1992; Blackwell 2000).

Furthermore, Alpert et al. (2004) semi-objectively categorized the daily synoptic systems that influence the EM and found that the Red Sea trough (RST) (or tropical-extratropical interaction) influences the rainfall patterns in the EM region, which was also confirmed in subsequent studies (Ziv et al. 2005; Haggag and El-Badry 2013; De Vries et al. 2013, 2016).

Previous works have indicated that rainfall over regions of interest is influenced directly by or through the effects of climate systems on local systems, but it has remained unclear how these local systems influence rainfall patterns. Therefore, the purpose of this study is to relate the northern AP (southern Levant) rain with the temporal and vertical variations in the STJ, which is one of the main local/regional atmospheric systems, over the Middle East and to detail the atmospheric characteristics that accompany the effects of STJ variability on winter rainfall over the northern AP.

This paper is organized as follows. The materials and methods used in this study are described in the “Materials and methods” section, the statistical results and synoptic

features of rain variability in winter months are presented and discussed in the “Results and discussion” section, and the conclusions are presented in the last section.

## Materials and methods

In this study, the STJ was detected using the method defined in Asiri et al. (2020), which specifies the STJ as the horizontal maximum wind on vertical levels from 400 to 200 hPa with a value greater than the threshold value close to 25 m/s (as used in Koch et al. 2006; Abish et al. 2015; Strong and Davis 2005, 2007) inside the area from 20°N to 50°N and from 00°E to 80°E; this region is considered one of the main cores of the STJ (Krishnamurti 1961; Strong and Davis 2007; Archer and Caldeira 2008).

The rain data were retrieved from surface rain observations at 15 surface meteorological stations in northern Saudi Arabia and adjacent areas through the period from 1978 to 2010 (Fig. 1b). This period was selected to include the longest possible records and minimal record gaps. The rain data were used to determine the rainfall cases (i.e., the days of precipitation greater than 1 mm at least at one station) and nonrainfall cases (i.e., the days with no rain observations at any of the surface stations).

Meteorological data were retrieved from the National Centers for Environmental Prediction (NCEP)/National Center for Atmospheric Research (NCAR) reanalysis 6-hourly meteorological data set during the period from 1978 to 2010, with a horizontal spatial resolution of  $2.5^\circ \times 2.5^\circ$  (Kalnay et al. 1996; Kistler et al. 2001). The study domain was delimited by 0°E–70°E and 10°N–50°N.

A synoptic evaluation of the composite maps of both rainfall and nonrainfall cases was performed based on the sea level pressure (SLP); the wind components at 850, 250, and 200 hPa; the vertical motion and geopotential heights at 850 and 700 hPa; and the relative humidity (RH) at 700 hPa. The static stability within the layer between 1000 and 500 hPa was calculated following the method of Gates (1961) for all selected composites.

The composite cases were detected depending on the rain threshold value and the corresponding times available for the jet classification, with vertical data for the highest STJ pressure levels and temporal data for winter months.

## Results and discussion

### General

The procedure used for detecting the STJs (Asiri et al. 2020) is shown in Fig. 1a, and 21300 STJs were found for the period from 1958 to 2016. Of these detected STJs, approximately

a)

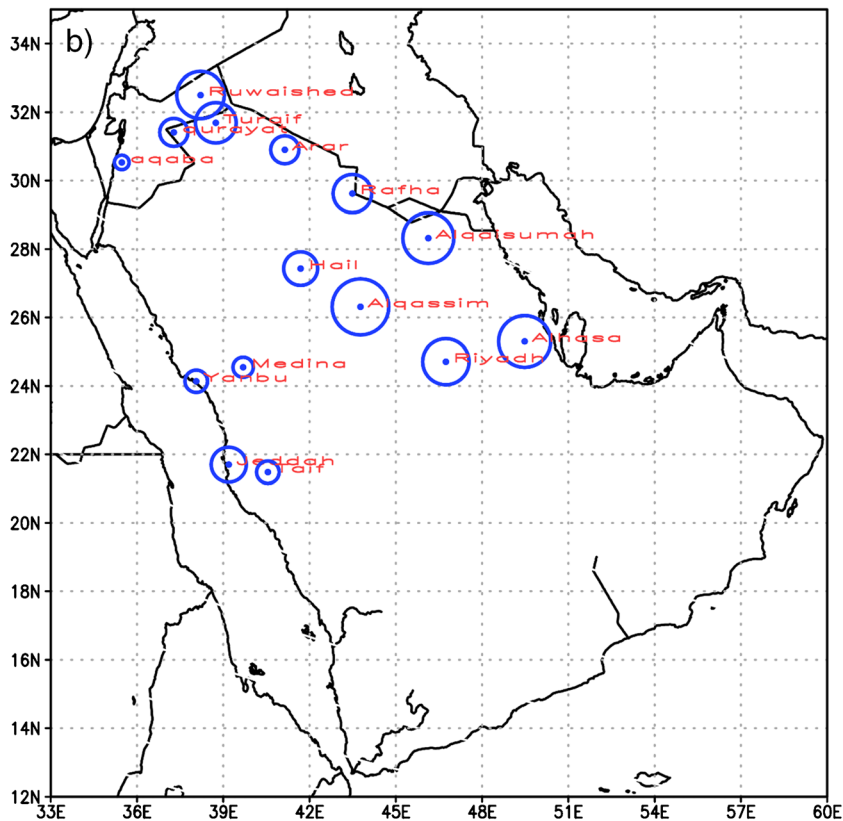
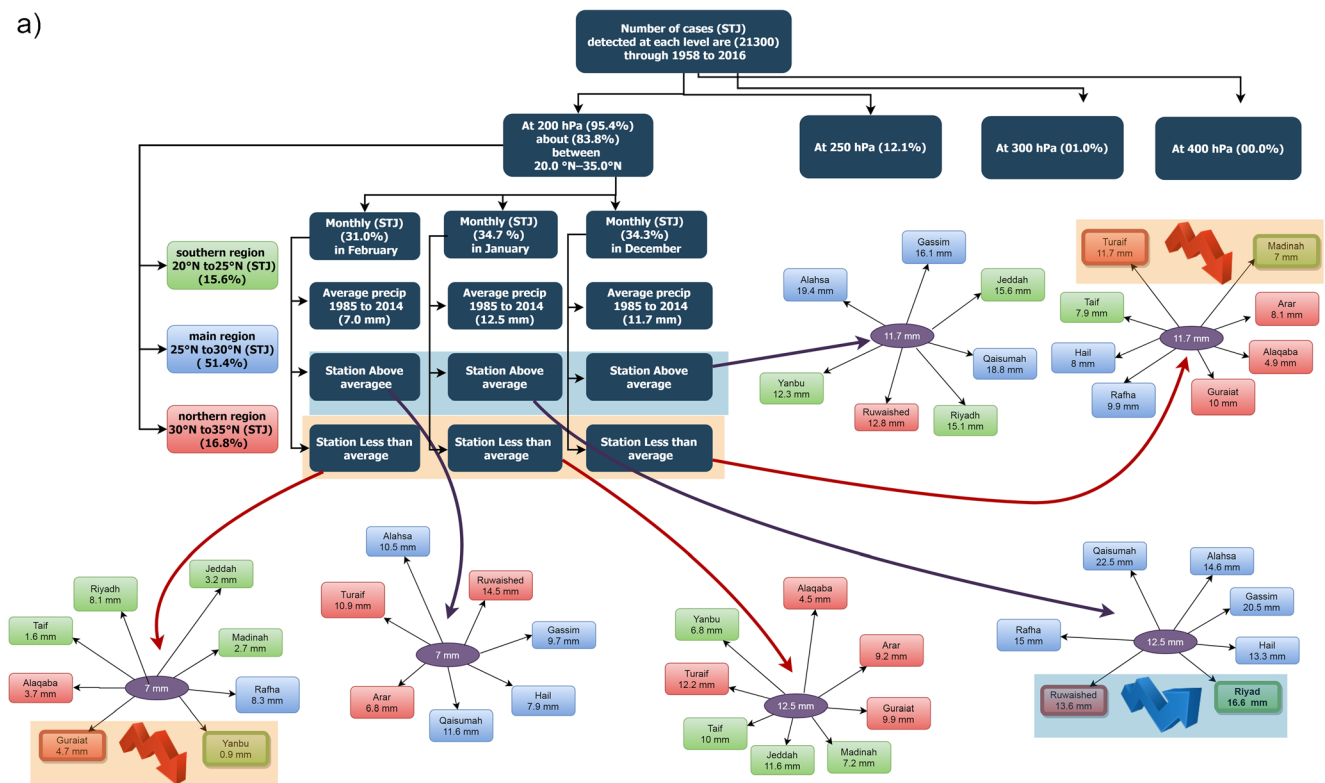


Fig. 1 Schematic distribution of the rainfall over the northern AP: a the regional and temporal distributions of the STJ and rainfall, b the horizontal distribution of rainfall at the 15 surface stations in the study region, and c the diurnal variations in the days of rainfall through the daytime hours (GMT)

c)

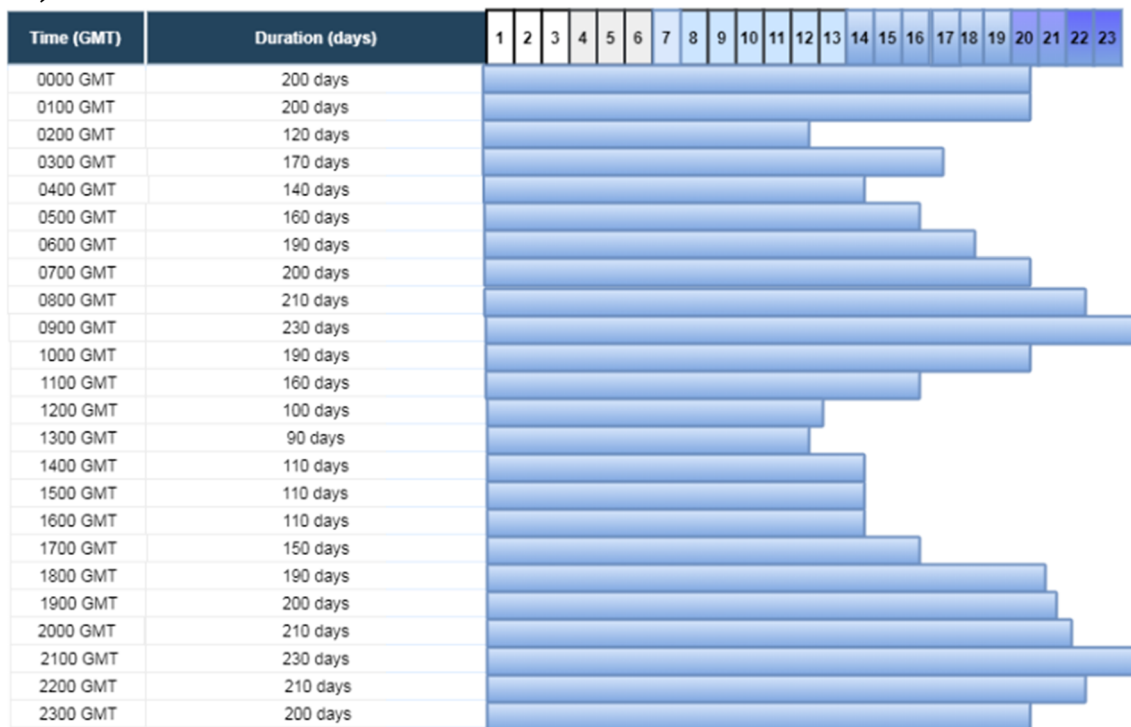


Fig. 1 (continued)

0.1% occurred at 300 hPa, 0.0% occurred at 400 hPa, approximately 12.1% occurred at 250 hPa, and 87.8% occurred at 200 hPa; i.e., most of the winter STJs were found at 200 hPa. Therefore, the STJs at 200 hPa were considered the climate STJ level for the winter in the Middle East region.

The spatial distribution of STJs at this level shows that approximately 95.4% of the detected STJs were found in the area between 20°N and 35°N, which represented 83.8% of the winter time. In detail, approximately 15.6% of the STJs occurred in the area between 20°N and 25°N, approximately 16.8% of the STJs occurred in the area between 30°N and 35°N, and approximately 51.4% of the STJs occurred in the area between 25°N and 30°N.

Temporally, the monthly detected STJs in the area between 20°N and 35°N show that approximately 34.3% occurred in December, 34.8% occurred in January, and 31.0% occurred in February.

The station rainfall distribution (Fig. 1b) shows that the highest rainfall was found over the eastern study region and over the northeastern stations, Ruwaished station (Jordan) and Turaif station, which is in agreement with the results reported by Mashat and Basset (2011). The lowest rainfall values were found at the western stations, with the overall lowest rainfall over the Aqaba station (Jordan).

Moreover, the average rain in the winter months increased from December to January and then decreased, with monthly averages of 11.7 mm, 12.1 mm, and 7.0 mm in December, January, and February, respectively. The annual average rain

in the area, at approximately 31 mm, was two orders of magnitude less than the annual average over Lebanon, which reached 546.5 mm (Kobrossi et al. 2021), or one order of magnitude less than the annual rain over all of Iran, which was approximately 240 mm (Raziei et al. 2005). However, it was comparable to the average rain over southeastern Iran, which was less than 20 mm (Ghasemi and Khalili 2008), and with the minimum annual value over Balochistan Province, Pakistan, which is classified between arid and hyperarid regions (Qaisrani et al. 2021). Although the average values for the months were 1° less than the average values over the southeastern Mediterranean, they were consistent with the monthly distribution (Saaroni et al. 2019; Ben-Gai et al. 1993) and greater than the minimum value of rain in the wet Mediterranean season, which was 15 mm (Dunkeloh and Jacobeit 2003), as well as the annual average (25 mm) for the wet season over southern Israel (Ziv et al. 2014). This result is compatible with the negative trend (dry) of the annual rainfall found in this region (Mashat and Abdel Basset 211). The highest rainfall amounts were most commonly found at the Al-Riyadh, Al-Hasa, Al-Gassim, and Al-Qaysumah stations in all winter months, all of which are located in the main region of the STJ, i.e., in the region between 25°N and 30°N. Additionally, the distribution of the rain indicated a greater decrease in the amount of rain as the STJ shifted southward than as the STJ shifted northward, while rain reached its maximum value when the STJ was located over the region between 25°N and 30°N.

The hourly rainfall time (Fig. 1c) indicated that most of the rainfall over the northern AP was produced between 12 GMT and 20 GMT, i.e., during the afternoon period, while no rain occurred in the morning from 00 GMT to 11 GMT, and little rainfall was produced between 21 GMT and 23 GMT, i.e., during the late afternoon.

Moreover, the monthly distribution of rainfall (Fig. 2) indicated that all months had decreasing rates after 1995, with a small rate of decrease in January and the highest rate of decrease in December and February. This trend was comparable to rainfall trends over Syria (Kelley et al. 2015), Lebanon (Kobrossi et al. 2021), and the northern Middle East (Iqbal et al. 2013) but was inverse to rainfall trends over southern Israel (Ben-Gai et al. 1994, 1998; Steinberger and Gazit-Yaari 1996). Generally, the monthly amounts of rain (Table 1) indicated that February had the highest (lowest) ratio of days with rainfall less (greater) than 10 mm (50 mm), while December was the month with the highest ratio of days receiving rainfall amounts greater than 50 mm.

### Synoptic climatology study (January)

The above discussion indicated that the area between 25°N and 30°N is highly affected by jets and winter rain. Therefore, the present study considered the characteristics of the rainfall composite data in this area as the reference (or the climate) situation for comparison with nonrainfall composite data to describe the characteristics of atmospheric systems that generate rain. To define the temporal variability of winter rain patterns, the climate situation was compared with the rainfall composite data of the other winter months, while the influence of the vertical variability of the jet on the rainfall situation was examined by comparing the climate situation with the jet at 250 hPa.

### Mean sea level pressure and STJs at a pressure level of 200 hPa

In the rainfall composite (Fig. 3a), the Sudan low pressure, with a value of 1010 hPa, has an RST to the east of the Red Sea and is then oriented southeast-northwest to the EM, which is similar to the wet composite for the southern Levant (Ziv et al. 2006; Ghasemi and Khalili 2008) or the wet RST

**Table 1** The number (ratio) of days with observed rainfall amounts less than 10 mm (i.e., less than half of the annual rainfall amount) and greater than 50 mm (i.e., approximately double the annual rainfall amount)

Month/Num. of days	Total	Less than 10 mm	More than 50 mm
December	298	198 (66.4%)	20 (6.7%)
<b>January</b>	<b>435</b>	<b>255 (58.6%)</b>	<b>21 (4.8%)</b>
February	234	182 (77.8%)	6 (2.6%)

(Tsvieli and Zangvil 2005). Additionally, the orientation of the RST explains the increased surface moisture intrusion into the region. The Azores high, with a value of 1022 hPa, has a ridge over the Mediterranean and northern Africa, extending to eastern Egypt. The Siberian high, with a value of 1030 hPa, has a high-pressure cell with a value of 1024 hPa over the Caspian Sea. The relationship between previous systems, i.e., high-pressure systems surrounding the RST, is similar to that described for rainy events by De Vries et al. (2016).

Furthermore, these systems interact and form two pressure gradient areas: the highest over eastern Africa between the Azores high and RST and the lowest over the Levant and Iran between the Siberian high and RST. Additionally, the STJ (Fig. 3a) has a core with a value of 117 knots and extends from central Egypt to Pakistan.

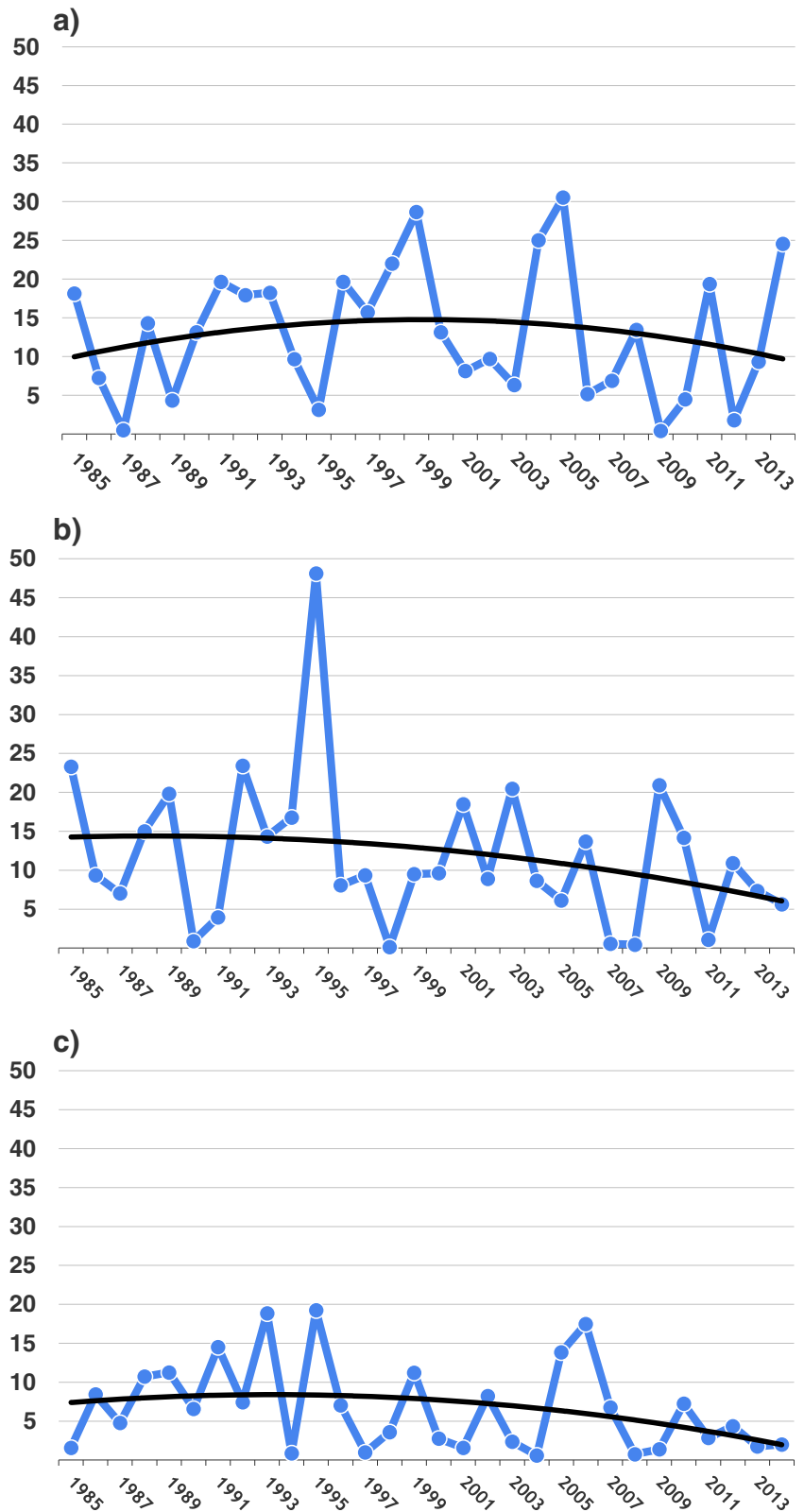
In comparison with the rainy composite, the nonrainfall composite (Fig. 3b) illustrates that the Sudan low does not change but shows the RST over the Red Sea and is not connected with the Mediterranean low pressure, with a value of 1018 hPa, which forms a situation similar to the composite of dry days for the southern Levant (Ziv et al. 2006). The Azores high does not change but has a ridge over northern Africa to mid-Libya. The Azores high is smaller in the nonrainfall composite, which shifts the pressure gradient area to the south. The change in the Azores high produces a negative effect on the rain over the northern AP compared to its positive effect on the rain situation over the northern Middle East (Iqbal et al. 2013). The Siberian high, with a value of 1028 hPa, has a high-pressure cell over the Caspian Sea with a value of 1024 hPa. The STJ (Fig. 3b) forms a zonal core with a value of 112 knots and extends from eastern Libya to the eastern AP.

The atmospheric systems for rainfall/nonrainfall SLP composites appear comparable to the wet/dry systems influencing Iran (Ghasemi and Khalili 2008) when considering their relationship with respect to the region's position. In the nonrainfall composite, the atmospheric systems interact and form weak gradient areas over eastern Africa, Iraq, and the northern Mediterranean, producing a weak atmospheric mechanism for rain.

### Geopotential height and vertical wind at 850 hPa

The rainy composite (Fig. 3c) shows that the northern cyclone, with a value of 1440 gpm, has a deep trough over the EM and northern AP. The subtropical anticyclone has two branches over Africa and the southeastern AP, each of which has a value of 1530 gpm. The African branch has a ridge over Africa to eastern Egypt and Sudan. The Arabian branch has a ridge oriented southeast to southwest over the southern AP, and the southwest wind influences the northern AP, with wind speeds decreasing from south to north and ranging from 10 to 5 knots.

**Fig. 2** Annual distribution of rainfall over the northern AP for **a** January, **b** December, and **c** February. The y-axis represents the rainfall days, and the black line is the trend line



The distribution of vertical motion (Fig. 3c) shows that there is high upward motion with a value of  $-0.8$  Pa/s over the southwest AP, while there are upward motions of

$-0.4$  and  $-0.2$  Pa/s over the Levant and central Mediterranean, respectively. The upward motion area is surrounded by areas of downward motion of  $0.6$  and  $0.4$

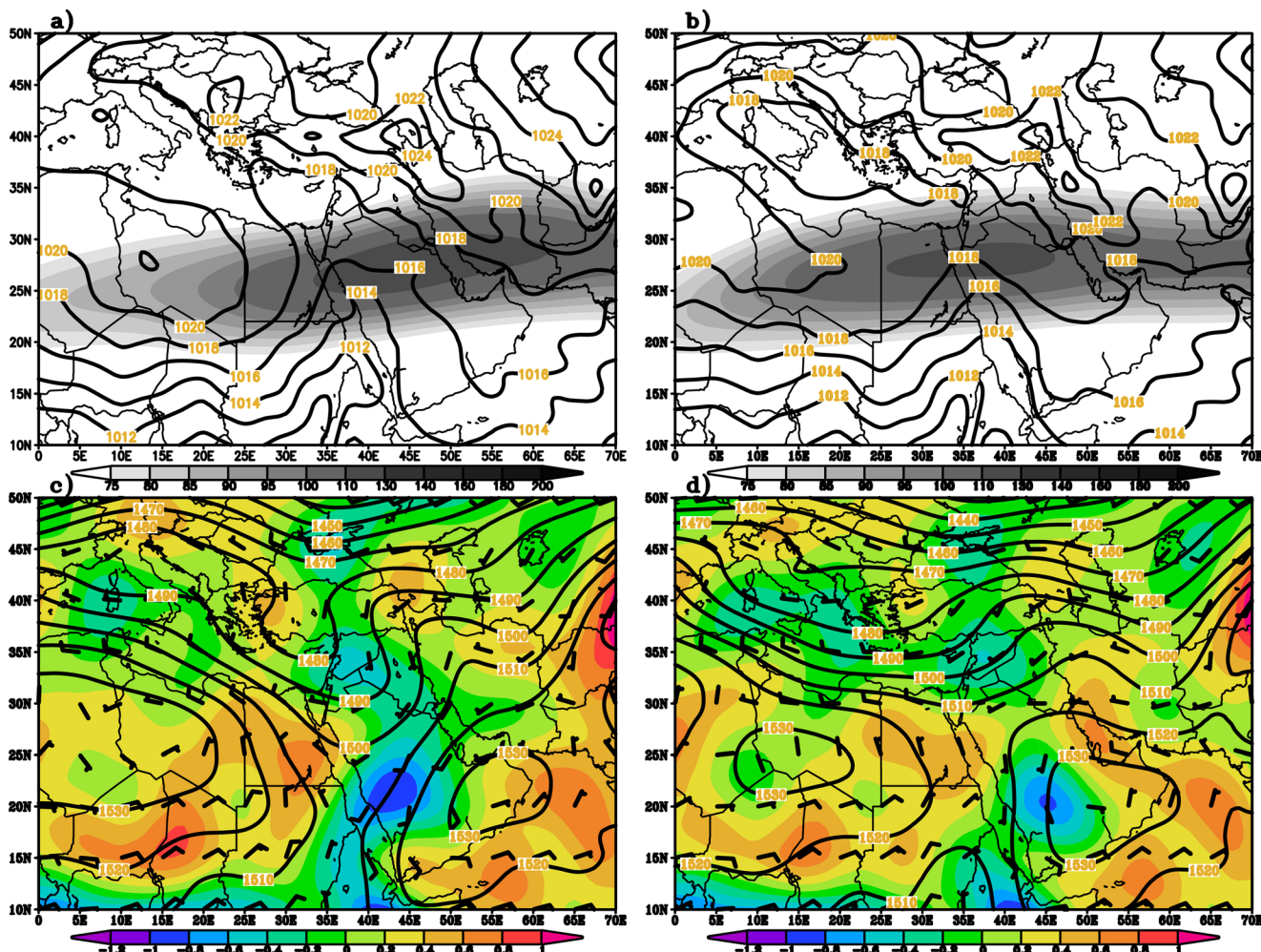


Fig. 3 Maps of the SLP (isobars, in hPa) and maximum wind at 200 hPa (shading, in knots) in January for a rainfall and b nonrainfall composites. Maps of the geopotential height (contours, in gpm), wind (barbs, in knots) and temperature (shading, in °C) at 850 hPa for January for c rainfall and d nonrainfall composites

Pa/s over northeast Africa and the area between the Caspian and Black Seas, respectively, which form a vertical circulation with downward branches outside the study area.

In comparison with the rainfall composite, the nonrainfall composite (Fig. 3d) shows that the northern cyclone deepens by approximately 10 gpm but has a wide trough over the EM and Levant. The subtropical anticyclone over Africa is more intense, with a value of 1540 gpm, and has a ridge over mid-Egypt and Sudan. The AP anticyclone with a value of 1530 gpm shifts westward and forms meridional contour lines over the western AP. The western wind influences the northern AP, and the wind speed is decreased compared to that of the rainfall composite. The wind directions accompanying the rainfall (nonrainfall) composite are similar to those of the wet (dry) composite over Iran (Ghasemi and Khalili 2008).

The vertical motion distribution (Fig. 3d) shows that the upward motion over the western AP and Levant is divided by an area of downward motion. A new area of upward motion with a value of  $-0.6$  Pa/s is generated over the northern Arabian Gulf, and the core of downward motion over northwestern Africa shifts northward over Egypt. The entire Mediterranean is influenced by upward motion, with the highest value of  $-0.4$  Pa/s over the eastern region; i.e., the vertical circulation shifts slightly out of the study area.

From the previous description of the synoptic features, the orientation of the Arabian anticyclone clearly plays an important role in the southward extension of the northern cyclone trough, which, in turn, substantially affects the generation of rainfall in the region by triggering and enhancing tropical convection (Kiladis and Weickmann 1992; Blackwell 2000; Ziv et al. 2006).

**Geopotential height at 500 hPa and static stability in the 1000–500 hPa layer**

At 500 hPa in the rainfall composite (Fig. 4a), the northern cyclone with a value of 5460 gpm has a deep trough over the EM and western Red Sea. The subtropical anticyclone with a value of 5860 gpm over the Arabian Sea has two ridges over the Arabian Gulf and over western Africa and the Mediterranean.

The wind at this level has its maximum at approximately 27.5°N, with the highest value of 50 knots over the central AP. The wind decreases northward and southward, but has a higher rate of decrease southward.

The stability distribution (Fig. 4a) shows that the low-stability area over the Mediterranean and African Horn areas, at  $0.9^{\circ} \text{ db}^{-1}$ , appears connected, while it is surrounded by a high-stability area over Africa, the Arabian Sea, and the

northern region, with a value of  $1.2^{\circ} \text{ db}^{-1}$ . This stability distribution forms stability gradients over the Red Sea, northern Africa and Mediterranean regions.

In the nonrainfall composite (Fig. 4b), the northern cyclone with a value of 5420 gpm has a trough oriented northeast to southwest over the central and western Mediterranean. The subtropical anticyclone with a value of 5860 gpm has a ridge over the western AP and Red Sea. This atmospheric system distribution is similar to the negative phase of the fourth mode (Dunkeloh and Jacobeit 2003) for dry conditions over the Levant and dry days over the southeastern Mediterranean (Saaroni et al. 2019). Although the wind speed decreases in this composite compared to the rainy composite, the maximum wind remains at approximately 27.5°N.

The distinction between the rainfall/nonrainfall troughs of the northern cyclone, i.e., oriented more north-south on the rainfall composite, is similar to the difference detected in the

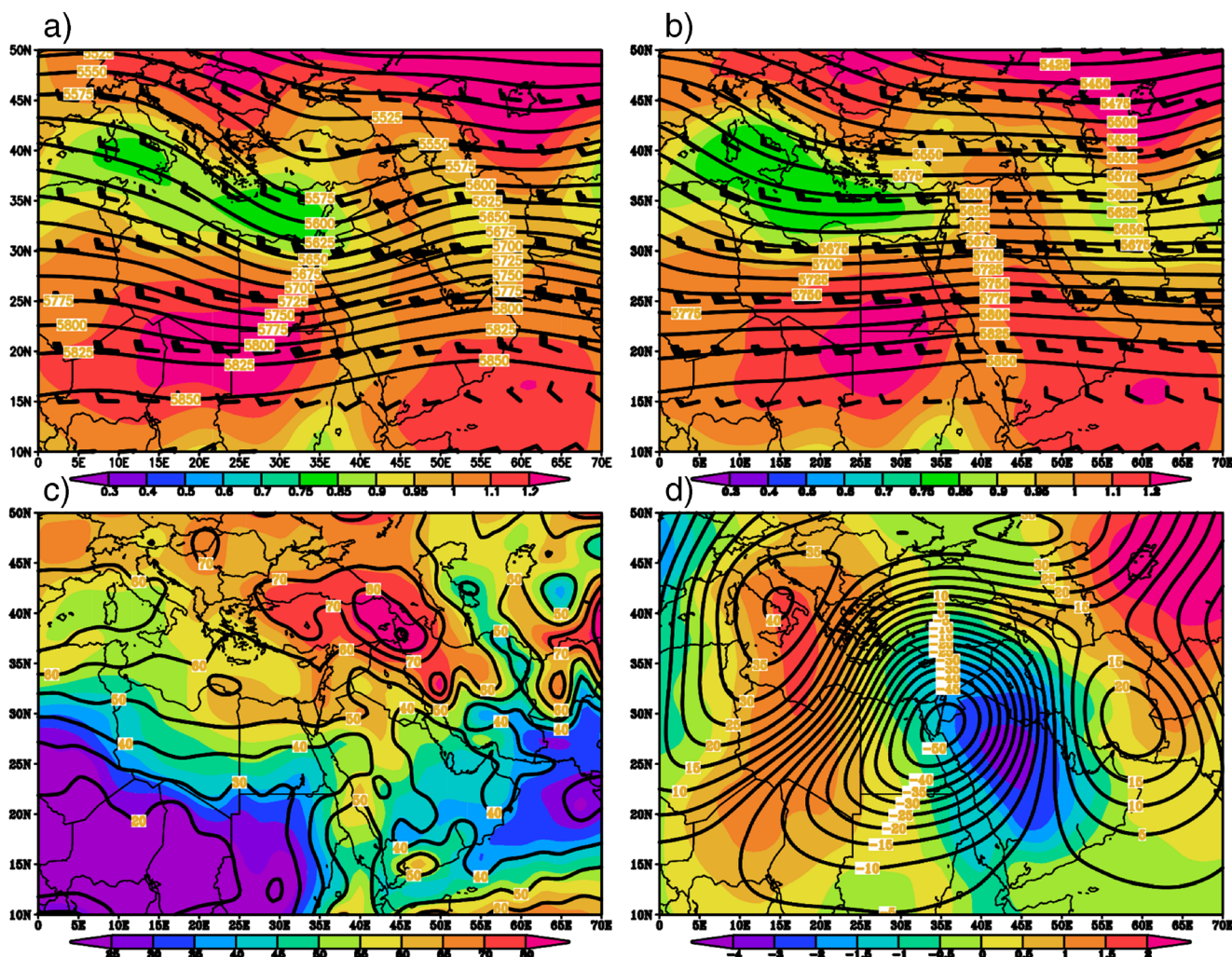


**Fig. 4** Maps of the geopotential height (contours, in gpm), wind (barbs, in knots), and temperature (shading, in °C) at 500 hPa in January for a rainfall and b nonrainfall composites. Maps of c the relative humidity in % (contours for nonrainfall and shading for rainfall) at 700 hPa and d the

difference in the SLP (shading, in hPa) between rainfall and nonrainfall composites and 500 hPa geopotential height (contours, in gpm) for the January composites



wet/day composites for the southern Levant and Iran and is explained as a factor enhancing the EM low pressure responsible for the rainfall system (Ziv et al. 2006; Ghasemi and Khalili 2008).

In the nonrainfall composite (Fig. 4b), the low stability over the Mediterranean has a value of  $0.8^{\circ} \text{ db}^{-1}$ , while the value over the African Horn reaches  $0.9^{\circ} \text{ db}^{-1}$ . The high-stability areas over the Arabian Sea extend northward and are connected with the African high-stability region, and both have a value of  $1.2^{\circ} \text{ db}^{-1}$ . This distribution tends to shift the Mediterranean low-stability area to over the EM region rather than southward, as in the rainfall composite. The stability gradient around the Red Sea decreases in the nonrainfall composite compared to that in the rainfall composite.

Generally, the above discussion indicates that the mechanisms accompanying the rainfall composite produce integrated atmospheric layers, i.e., the upper trough to the western lower trough with low stability and clear vertical circulation, which enhances the factors conducive to rainfall (Kiladis and Weickmann 1992; Blackwell 2000; Ziv et al. 2006).

#### Relative humidity at 700 hPa and SLP/500 hPa geopotential differences

In the rainfall composite (Fig. 4c), the distribution of RH shows values between 60 and 70% over the northern AP and Levant, while the highest value of 90% appears over the area between the Caspian and Black Seas. Additionally, a high moisture content between 50 and 60% is found over the eastern Red Sea and western AP.

In the nonrainfall composite (Fig. 4c), the northern AP and Levant have RH values between 40 and 60%, and the highest RH value, 90%, is located in the area between the Caspian and Black Seas. The highest RH over the Red Sea is found in the southern region, with a value of 50%.

The SLP difference (Fig. 4d) has a negative core with a value of  $-3.5 \text{ hPa}$  located over the northern AP, and difference lines are oriented south to north on the western side and are wavy on the eastern side. Two areas of positive difference are found in the western and eastern regions, with values of  $1.5 \text{ hPa}$  and  $2.5 \text{ hPa}$ , respectively. The western region has a high-difference core over the Mediterranean and forms a meridional SLP difference gradient from north to south through the EM and Red Sea. The eastern region has a core over the eastern corner and forms a zonal SLP difference gradient over the Levant.

At 500 hPa (Fig. 4d), the negative geopotential height difference with a value of  $-50 \text{ gpm}$  is located over the northern Red Sea, i.e., to the west of the surface difference. This negative difference is surrounded by positive difference areas, with the highest value of  $40 \text{ gpm}$  located over Italy. The interactions between different areas form a high geopotential difference gradient over Africa and the AP. Moreover, the

different distributions of SLP and geopotential heights are similar to those during the wet season in January over the EM (Tsvieli and Zangvil 2005).

In an integrated form, the results show that the distributions of vertical motion and stability, in addition to the northward extended RST and its deep interaction with the upper trough, lead to a destabilized troposphere and form rain over the AP (Barth and Steinkohl 2004; Evans et al. 2004; Chakraborty et al. 2006; Evans and Smith 2006; De Vries et al. 2016). The rainy system conditions appeared similar to those that produce rain over Iran (east and southeast of the study area) (Ghasemi and Khalili 2008), while the distribution of the geopotential differences appears similar to those for high/low rainfall over the EM region (Eshel and Farrell 2000; Krichak et al. 2000).

#### Temporal variability

In this part, the synoptic discussion is constrained only to rainfall/nonrainfall cases observed in the area between  $25^{\circ}\text{N}$  and  $30^{\circ}\text{N}$  and accompanied by the jet at 200 hPa, and these conditions are all fixed except the temporal (i.e. monthly) variation.

#### December

##### Mean sea level pressure and STJ at a pressure level of 200 hPa

For the rainfall composite (Fig. 5a), the Sudan low with a value of 1006 hPa has an RST over the Red Sea extending northward to approximately  $30^{\circ}\text{N}$ . The northern Mediterranean is influenced by a weak low-pressure system with a value of 1010 hPa over Italy. The southeastern Mediterranean is influenced by a high-pressure cell with a value of 1014 hPa that forms a wide weak ridge over northern Africa and the central northern AP. The Siberian high with a value of 1018 hPa has a high-pressure cell over the area between the Caspian and Black Seas and a ridge over Iran and the northern Arabian Gulf. The STJ, with a value of 90 knots, has a core extending from Algeria to western Egypt, and has a trough shape over the northern Red Sea and a ridge shape over the AP.

For the nonrainfall composite (Fig. 5b), the Sudan low does not change but exhibits a relatively flat RST over the eastern Red Sea with an eastward orientation in contrast to the rainfall composite. The Azores high pressure over the Mediterranean and northern shore of Africa with a value of 1014 hPa extends to the EM and has a wide ridge over Africa. The Siberian high pressure with a value of 1020 hPa has a cell in the area between the Caspian and Black Seas and forms a pronounced ridge over Iran. The STJ core stretches between eastern Algeria and the Red Sea, with a value of 89 knots, and forms a trough shape over the Levant (Fig. 5b).

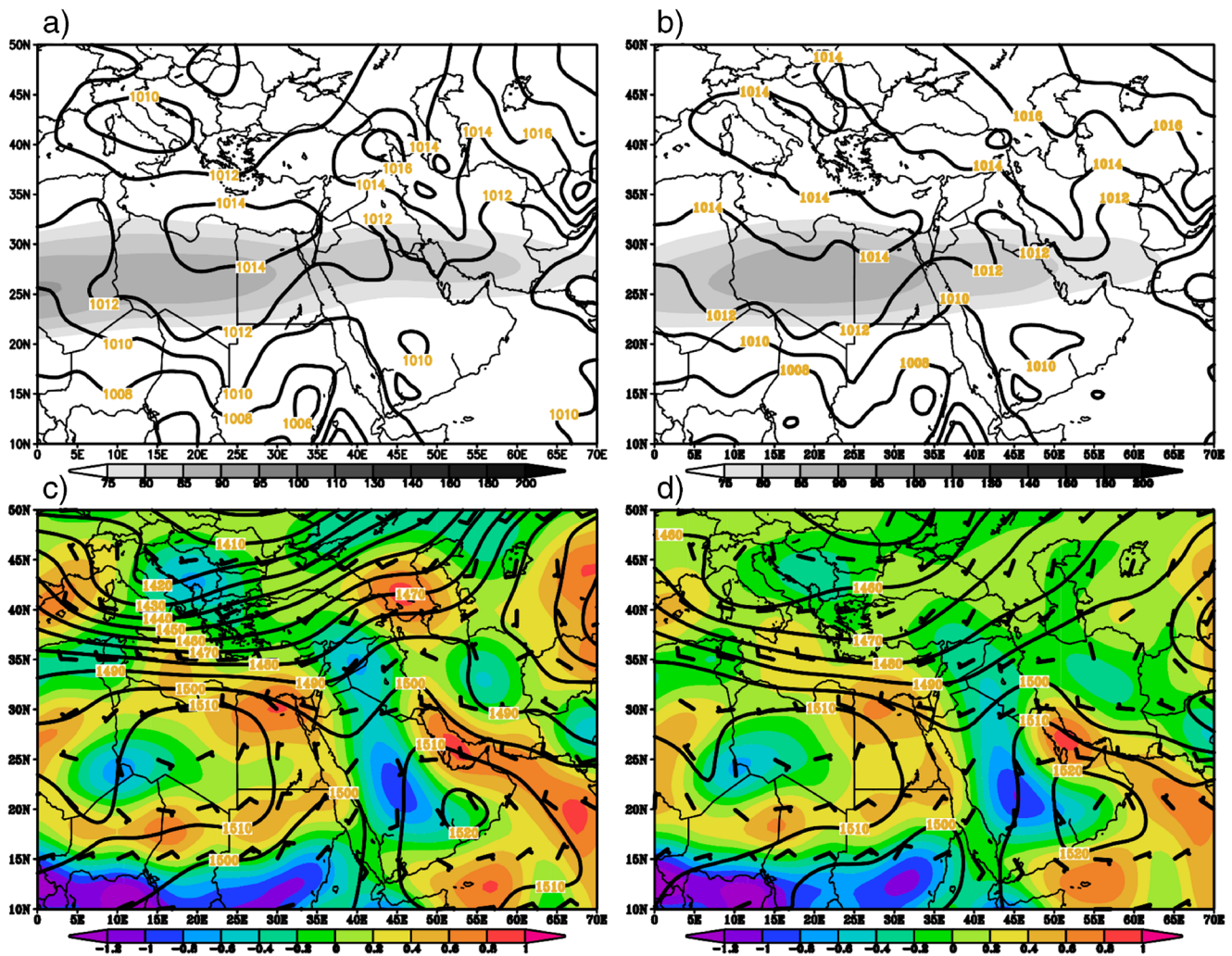


**Fig. 5** Maps of the SLP (isobars, in hPa) and maximum wind at 200 hPa (shading, in knots) in December for **a** rainfall and **b** nonrainfall composites. Maps of the geopotential height (contours, in gpm), wind

(barbs, in knots) and temperature (shading, in °C) at 850 hPa in December for **c** rainfall and **d** nonrainfall composites

**Geopotential height and vertical wind at 850 hPa** In the rainy composite (Fig. 5c), the northern cyclone with a value of 1400 gpm has a high-gradient flat trough over the central Mediterranean and over the eastern and northern AP. The tropical cyclone with a value of 1500 gpm extends northward over the Red Sea to approximately 22°N. The subtropical anticyclone over Africa has a cell over Egypt and Libya, with a value of 1510 gpm, and a ridge extending eastward to mid-Egypt. The subtropical anticyclone cell over the southern AP with a value of 1520 gpm has a ridge over the eastern AP. The wind speed decreases from south to north over the western AP, with values ranging from 10 to 5 knots.

The highest upward motion,  $-0.8$  Pa/s, is found over the southern AP and extends northward to Turkey (Fig. 5c). This upward motion is surrounded by two cores of downward motion: one core with a value of  $0.6$  Pa/s is over Egypt, and the other core with a value of  $0.8$  Pa/s is over the Arabian Gulf. This distribution forms a vertical motion gradient across the

Red Sea and Arabian Gulf, with a maximum gradient area around the EM and northern AP.

In the nonrainfall composite (Fig. 5d), the northern cyclone with a value of 1450 gpm has a flat trough over the EM and northwestern AP. The tropical cyclone with a value of 1500 gpm has a trough over southern Sudan, i.e., southward on the rainy composite. The subtropical anticyclone over Africa weakens, with a value of 1510 gpm, and its ridge extends eastward to Egypt, i.e., to the west of its location in the rainy composite. The AP anticyclonic cell with a value of 1520 gpm shrinks to the eastern AP.

In Fig. 5d, the maximum core of upward motion, with a value of  $-0.9$  Pa/s, forms over the southern AP and has a lower gradient on its northward extension than the core in the rainy composite. Although the intensity of downward motion over Egypt is comparable to the downward motion in the rainfall composite, there is a smaller gradient over the EM and northern AP in the nonrainfall composite.

**Geopotential height at 500 hPa and static stability at the 1000–500 hPa layer** In the rainfall composite (Fig. 6a), the northern cyclone, with a value of 5480 gpm, has a flat gradient trough over the EM and eastern Africa. The subtropical anticyclone, with a value of 5860 gpm, has a ridge over the AP. The wind speed at this level reaches its maximum value of 30 knots over the central and northern AP and decreases northward and southward, with a high rate of decrease in the southward direction.

Figure 6a shows the low-stability area over the AP, with a value of  $0.7^\circ \text{ db}^{-1}$ , surrounded by two highly stable areas over the northern study region and over the Arabian Sea. The stable area over the EM, with a value of  $0.85^\circ \text{ db}^{-1}$ , along with the low-stability area over the northern AP, forms a stable gradient area over the Levant and northern Red Sea.

In the nonrainfall composite (Fig. 6b), the northern cyclone, with a value of 5530 gpm, has a relatively weak flat gradient trough over the EM and Africa. The subtropical anticyclone, with a value of 5860 gpm, has a ridge over the AP. The distribution of the previous atmospheric systems is similar to that of baroclinic dry days over the southeastern Mediterranean (Saaroni et al. 2019). The wind speed distribution reaches its maximum value of 35 knots over the northern AP and decreases at the same rate in the rainy composite to the north and south.

In Fig. 6b, there is a stability gradient area over the Levant and northern Red Sea between the high-stability area over the EM and the low-stability area over the Levant and northern AP, and the stability lines have orientations that appear to the west of those in the rainfall composite.

The RST is one of the atmospheric systems considered to be associated with dry/wet EM systems (Krichak et al. 2000). However, the above discussion demonstrates that the atmospheric systems during rainy situations—i.e., the northward extension of the trough from the upper tropical cyclone, the upward motion, the low-stability area and the gradient areas of pressure, geopotential, stability and vertical motion—provide favorable conditions for the RST to become pronounced and extend northward, which forms a destabilized atmosphere (e.g. Evans and Smith 2006; De Vries et al. 2016) that achieves suitable conditions for rainfall. In contrast, the system pattern is not sufficiently clear during the nonrainfall cases.

**Relative humidity at 700 hPa and SLP/500 hPa geopotential differences** In the rainfall composite (Fig. 6c), the northwestern corner of the AP has a range of RH between 30 and 40%, while the northeastern corner has a range between 30 and 50%. The central part of the northern AP has an RH value of approximately 30%.

Although the RH over the northeastern corner of the AP in the nonrainfall composite (Fig. 6c) is comparable to the RH in the rainfall composite, the northwestern corner appears to be

dry. The central northern AP has an RH of approximately 10%, which is lower than the RH in the rainfall composite.

At SLP, positive difference cells (Fig. 6d) are distributed from central Africa to the east, and the two cores with the highest difference are found over Turkey and the northeastern region, with a value of 1.0 hPa. The highest negative difference reaches  $-5.0$  hPa, is located over the northern region, and forms SLP differences with a wavy shape over eastern Europe and northwestern Asia. Generally, a very weak difference in SLP appears over the EM, Levant and northern AP.

At 500 hPa (Fig. 6d), the highest negative geopotential difference of  $-75$  gpm is located over northern Europe. The highest positive difference, with a value of 20 gpm, is located over the northeastern corner of the study region. Moreover, the highest geopotential difference gradient is formed over Europe, while a weak geopotential gradient is formed over the Levant and northern AP.

This distribution indicates that in the rainy composite, there is deep low pressure over Europe, a relatively sharp trough over the northern AP and the Levant, and an extension of the subtropical anticyclone over AP.

## February

### Mean sea level pressure and STJ at a pressure level of 200 hPa

In the rainfall composite (Fig. 7a), the Sudan low, with a value of 1010 hPa, has an RST over the Red Sea and is not connected with the Mediterranean low pressure, which has a value of 1018 hPa. The Azores high, with a value of 1022 hPa, has a ridge over northern Africa and extends to mid-Libya. The Siberian high, with a value of 1028 hPa, has a high cell with a value of 1024 hPa over the area between the Caspian and Black Seas. These systems form pressure gradient areas around the Red Sea, Iraq, Iran, and southern Europe. The STJ (Fig. 7a) has a core with a value of 116 knots and extends from eastern Libya to eastern Iran; i.e. the STJ is strengthened by approximately 26 knots from its value in December.

In the nonrainfall composite (Fig. 7b), the atmospheric systems appear similar to those in the rainfall composite, except that the Azores high weakens to 2 hPa and shifts southward and the Mediterranean low extends throughout the Mediterranean. Additionally, the STJ core becomes zonal, with a value of 116 knots, and shrinks (Fig. 7b), extending from eastern Egypt to the eastern AP; i.e., its exit is located over the northeastern AP rather than outside of the AP, as in the rainfall composite.

### Geopotential height and vertical wind at 850 hPa

In the rainfall composite (Fig. 7c), the northern cyclone, with a value of 1440 gpm, has a deep trough over the EM and northern Red Sea. The tropical cyclone, with a value of 1510 gpm, has a trough over Somalia. The subtropical anticyclone has

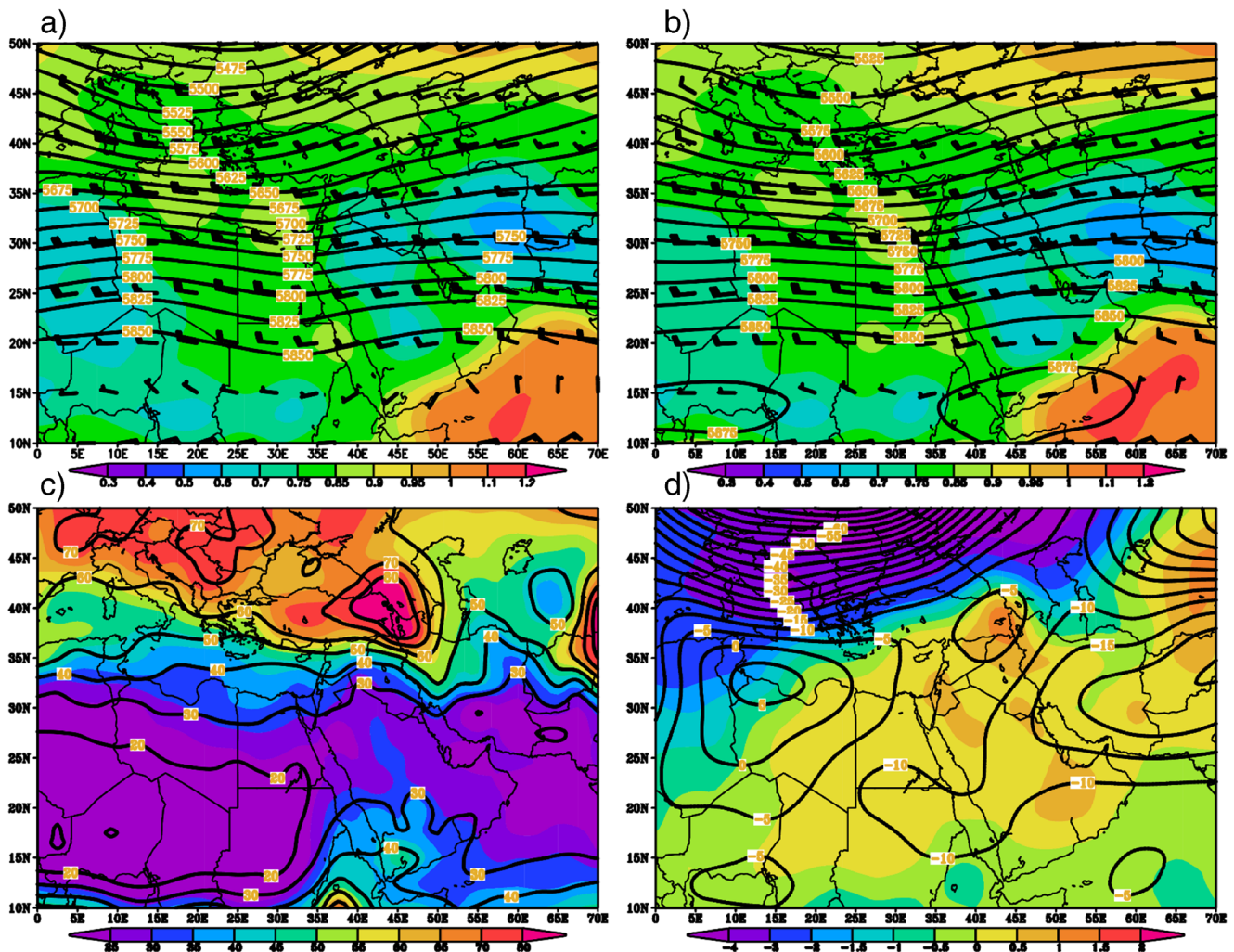


**Fig. 6** Maps of the geopotential height (contours, in gpm), wind (barbs, in knots) and temperature (shading, in °C) at 500 hPa in December for a rainfall and **b** nonrainfall composites. Maps of **c** the relative humidity in % (contours for nonrainfall and shading for rainfall) at 700 hPa and **d** the

difference in the SLP (shading, in hPa) between rainfall and nonrainfall composites and 500 hPa geopotential height (contours, in gpm) for the December composites

two branches: a branch over Africa, which extends eastward to western Egypt and Sudan and has a value of 1540 gpm, and a branch over the AP, which extends over the eastern AP and has a value of 1530 gpm. The wind speed at this level is highest over the southern AP, Red Sea, and Arabian Gulf, with a value of 10 knots, while it is lowest elsewhere over the AP, with a value of 5 knots.

The upward motion (Fig. 7c) has a maximum value of  $-1.0$  Pa/s over the southern AP, which appears as a continuation of tropical upward motion. Additionally, the upward motion extends northward over the AP and has a new core value of  $-0.4$  Pa/s over the Levant and a value of  $-0.2$  Pa/s eastward over Iran. The upward motion over the AP is surrounded to the west, north, and south by areas of downward motion, with values of 0.6, 0.2, and 0.8 Pa/s, respectively. In the western region, downward motion combines with upward motion over the AP to produce a vertical motion gradient area over the

western AP and EM. The southern downward motion combines with upward motion, producing a high vertical motion gradient over the southern region. However, the northern downward motion forms a weak vertical motion gradient over the northern Levant.

Although the atmospheric systems of the nonrainfall composite (Fig. 7d) appear similar to those of the rainfall composite, the trough of the northern cyclone shrinks northward and becomes sharp, and the ridge of the subtropical anticyclone over the AP shifts northwestward.

In the nonrainfall composite (Fig. 7d), the downward motion over eastern Africa, which appears in the rainy composite, shifts eastward and has a core value of 0.6 Pa/s over the Red Sea. A new high downward motion, with a value of 0.8 Pa/s, appears over the Arabian Gulf and, with the Red Sea downward motion area, forms a belt of downward motion separated by the southern upward motion, with a value of  $-0.8$  Pa/s, and

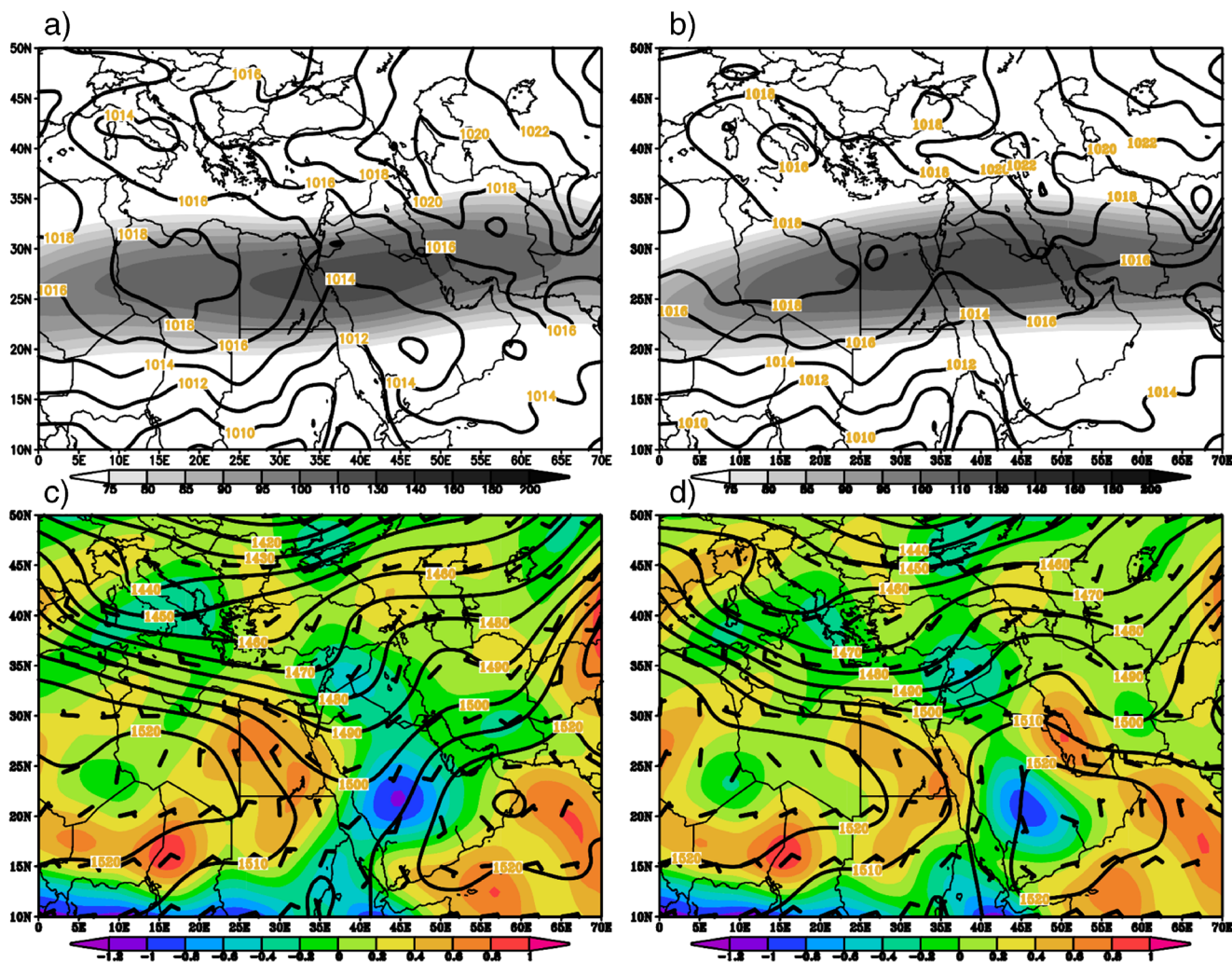


Fig. 7 Maps of the SLP (isobars, in hPa) and maximum wind at 200 hPa (shading, in knots) in February for a rainfall and b nonrainfall composites. Maps of the geopotential height (contours, in gpm), wind (barbs, in knots)

and temperature (shading, in °C) at 850 hPa for February for c rainfall and d nonrainfall composites

by the Levant upward motion, with a value of  $-0.4 \text{ Pa/s}$ . The previous distribution of vertical motions produces an area with a vertical motion gradient south of the rainy composite, relatively far from the northern region and EM.

**Geopotential height at 500 hPa and static stability in the 1000–500 hPa layer**

In the rainfall composite (Fig. 8a), the northern cyclone, with a value of 5420 gpm, has a trough over the central Mediterranean and western Africa. The subtropical anticyclone, with a value of 5860 gpm, has a ridge over the AP. The wind speed at this level has a maximum value at approximately 25°N and decreases northward and southward, with the highest rate of decrease southward.

The stability (Fig. 8a) forms a belt of low stability over the Mediterranean, with a value of  $0.8^\circ \text{ db}^{-1}$ , and over Iran, with a value of  $0.85^\circ \text{ db}^{-1}$ . In addition, a relatively low-stability area,

with a value of  $0.9 \text{ db}^{-1}$ , is located over the southern AP. High-stability areas with a value of  $1.1^\circ \text{ db}^{-1}$  are located over Africa and over the Arabian Sea and, with the low-stability belt, form areas with stability gradients around northern Africa and the Red Sea and over the southern AP and Arabian Gulf, respectively. Furthermore, the Mediterranean low-stability area extends to the Levant and the northern AP and has a value of  $0.85^\circ \text{ db}^{-1}$ .

In the nonrainfall composite (Fig. 8b), the atmospheric features appear similar to those in the rainfall composite, but the trough of the northern cyclone flattens and shrinks northward, and the ridge over the AP is more pronounced. This situation is similar to that on subtropical dry days (Saaroni et al. 2019) over the southeastern Mediterranean.

The low stability over the Mediterranean, with a value of  $0.75^\circ \text{ db}^{-1}$  (Fig. 8b), extends to the Levant and is connected with the low-stability region over the northern AP, which has a value of  $0.95^\circ \text{ db}^{-1}$ . Additionally, the low-stability region

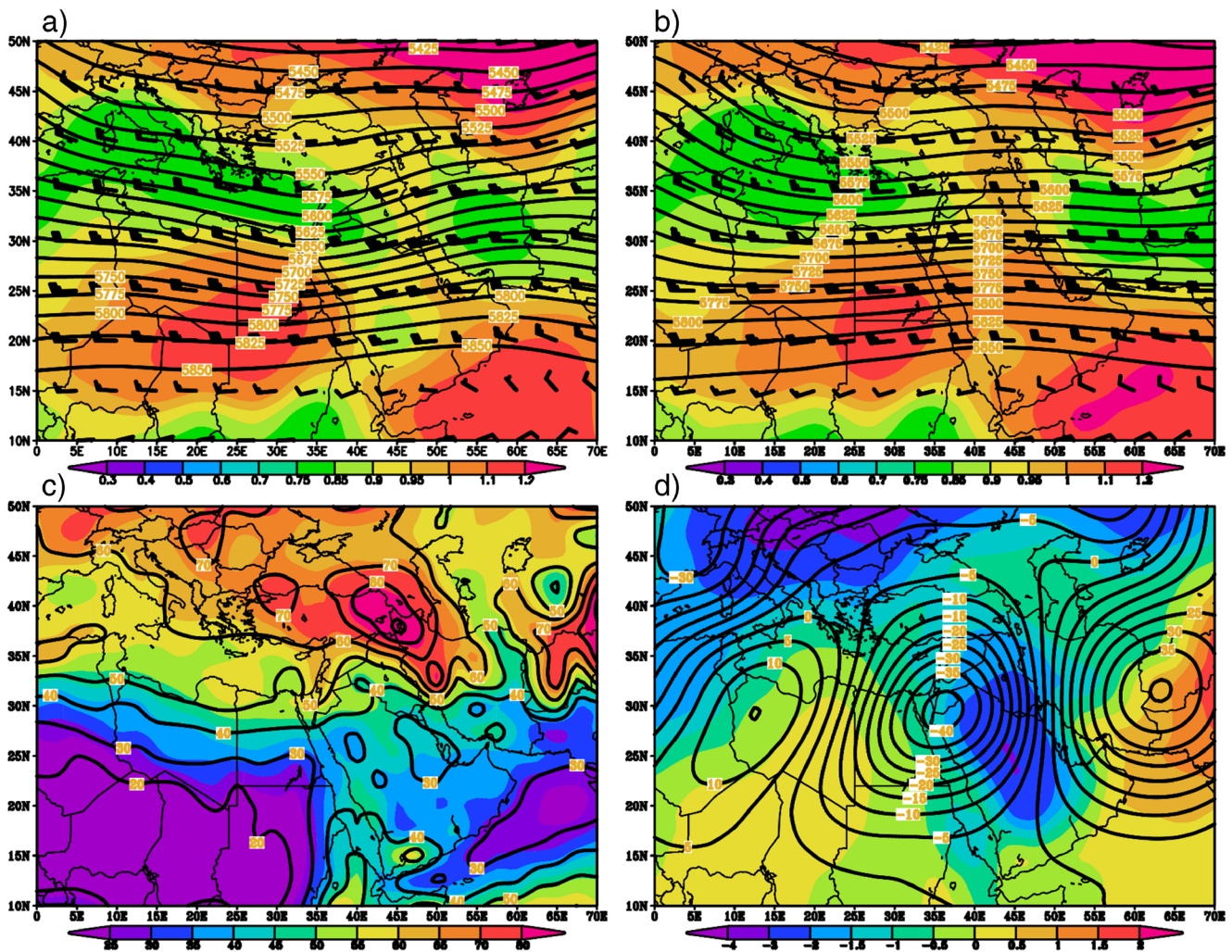


**Fig. 8** Maps of the geopotential height (contours, in gpm), wind (barbs, in knots), and temperature (shading, in °C) at 500 hPa in February for a rainfall and b nonrainfall composites. Maps of c the relative humidity in % (contours for nonrainfall and shading for rainfall) at 700 hPa and d the

difference in the SLP (shading, in hPa) between rainfall and nonrainfall composites and 500 hPa geopotential height (contours, in gpm) for the February composites

over Iran, with a value of  $0.8^{\circ} \text{ db}^{-1}$ , extends northwest to the Caspian Sea. The high-stability region over eastern Africa and the AP with a value of  $1.1^{\circ} \text{ db}^{-1}$ , together with the low-stability region over the Mediterranean and Levant, forms a stability gradient area over northern Africa and over the Arabian Gulf.

**Relative humidity at 700 hPa and SLP/500 hPa geopotential differences** In the rainfall composite (Fig. 8c), the moisture over the northern AP and Levant ranges between 50 and 60%. Additionally, as in the previous months, the highest moisture of 90% is found over the area between the Caspian and Black Seas. The peak moisture associated with the Red Sea is found over the southern Red Sea and has a value of less than 50%.

In the nonrainfall composite (Fig. 8c), the northern AP and Levant show RH values ranging from 40 to 50%, and the Red

Sea has a moisture content of approximately 40%, i.e., less than 10% of that of the corresponding areas in the rainfall composite.

Over the whole area (Fig. 8d), the SLP difference has negative cores over the AP, northern Europe and the eastern corner of the area, with values of  $-3 \text{ hPa}$ ,  $-3.5 \text{ hPa}$ , and  $-2.5 \text{ hPa}$ , respectively. Two weak positive differences with values greater than  $0.0 \text{ hPa}$  and  $1.5 \text{ hPa}$  are located over central Africa and India, respectively. Generally, the difference lines are oriented north to south over the western AP and zonally over southern Europe. Additionally, the SLP difference exhibits a lower gradient and has a relatively short wave compared with the SLP difference in January.

At 500 hPa, the highest negative geopotential height difference, with a value of  $-40 \text{ gpm}$  (Fig. 8d), is located over the northwestern AP, while the highest positive differences over

the eastern region, with a value of 40 gpm, are over Afghanistan.

The previous distribution forms a geopotential difference gradient over Africa, the EM and the AP. Moreover, the maximum negative geopotential difference over the AP is located to the northwest of the SLP maximum negative difference.

Generally, the SLP difference and monthly average rain indicate that the amount of rain increases as the pressure gradient increases (and vice versa) or as the negative difference between rainfall and nonrainfall composites increases and spreads over the northern region, similar to the results for rainfall in Iran (Ghasemi and Khalili 2008). The rainy composite characteristics indicate the importance of the atmospheric mechanisms for the development of rainfall situations, such as the relative positions of the surface and upper troughs, stability and vertical motion cells.

In the main rainfall month (January), the RST extended northward and was oriented eastward to the EM with respect to the nonrainfall composite; furthermore, the STJ was not zonal and appeared to be oriented northward on its eastern side, similar to the wet composite over the southern Levant (Ziv et al. 2006), and exited out of the area of interest.

In the relatively low-rainfall month of December, the high-pressure systems were pronounced and accompanied by a high-strength gradient, which was considered an atmospheric factor contributing to the low rainfall in the region, especially the Siberian high (Kutiel 1991), while the cyclone systems shrank or had weakened gradients, and the STJ core shrank westerly, which formed an exit region over the AP.

In the low-rainfall month of February, the RST was located to the east and did not have a pronounced connection with the Mediterranean low pressure, and the Siberian high ridge extended westward in comparison with that in January.

Generally, the moisture distribution in different situations showed that the rainfall composite was greater than that of the nonrainfall composite, not less than 20% of it, except in December, when this value reached only 10%. Furthermore, the monthly distribution showed that the moisture in the January rainfall composite was larger than that in the month with the second highest value, February, by at least 10%, and the difference reached more than 40% in December.

### Vertical variability (STJ at 250 hPa)

This section describes the atmospheric features of the rainfall composite when the January jet is located at 250 hPa instead of the climate level of 200 hPa, which reflects the differences in rainfall atmospheric systems with the vertical variation in the jet.

### Mean sea level pressure and STJ at a pressure level of 250 hPa

In the rainy composite (Fig. 9a), the Sudan low, with a value of 1010 hPa, has an RST over the eastern Red Sea and extends northward to the EM. A weak low-pressure cell, with a value of 1018 hPa, is located over the EM but is not connected with the RST. The Siberian high, with a value of 1030 hPa, has a high-pressure cell, with a value of 1026 hPa, between the Caspian and Black Seas and forms a weak ridge over the Arabian Gulf and the Levant. The Azores high, with a value of 1024 hPa, has a wide ridge over northern Africa. The above systems interact and form two pressure gradient areas: a strong one over the western Red Sea and a weak one over the eastern Red Sea.

The STJ (Fig. 9a) has a trough shape over the Red Sea, and the core, with a value of 104 knots, extends from the east Red Sea to India.

In the nonrainfall composite (Fig. 9b), the Sudan low does not change, but the RST extends to the EM and the Levant. The Siberian high weakens, decreasing by 2 hPa, and the high-pressure cell between the Caspian and Black Seas has a pronounced ridge over the AP. The Azores high strengthens by 2 hPa and has a weak ridge over northern Africa. The effectiveness of the Azores high weakness has previously been reported (Saaroni et al. 2019; Raymond et al. 2018) for dry systems affecting the EM. The STJ (Fig. 9b) forms a ridge shape over the Red Sea, and its core, with a value of 112 knots, extends from Libya to India.

The previous systems interact and form two areas with different gradients around the Red Sea, with the highest located in the east.

### Geopotential height and vertical wind at 850 hPa

In the rainy composite (Fig. 9c), the northern cyclone, with a value of 1440 gpm, has a deep trough over the EM, northern AP, and Red Sea. The subtropical anticyclone has two branches over Africa and the AP. The African branch, with a value of 1540 gpm, has a ridge over the Mediterranean and Africa. The AP branch, with a value of 1530 gpm, has a ridge over Iran and Iraq. The wind speed weakens over the northern AP and increases in the surrounding areas.

An upward motion with a value of  $-1$  Pa/s (Fig. 9c) is located over the southern AP and extends over the Levant, with a value of  $-0.4$  Pa/s, and over the Mediterranean, with a value of  $-0.2$  Pa/s. This upward motion appears to be connected with tropical upward motion, with a value of  $-1.0$  Pa/s. Moreover, an area of upward motion, with a value of  $-0.4$  Pa/s, is located over the Black Sea. This area of upward motion is surrounded by areas of downward motion over Egypt and Sudan, with a value of  $0.6$  Pa/s. Furthermore, an area of downward motion over Italy and the northern Mediterranean has a value of  $0.8$  Pa/s. These areas of upward and downward

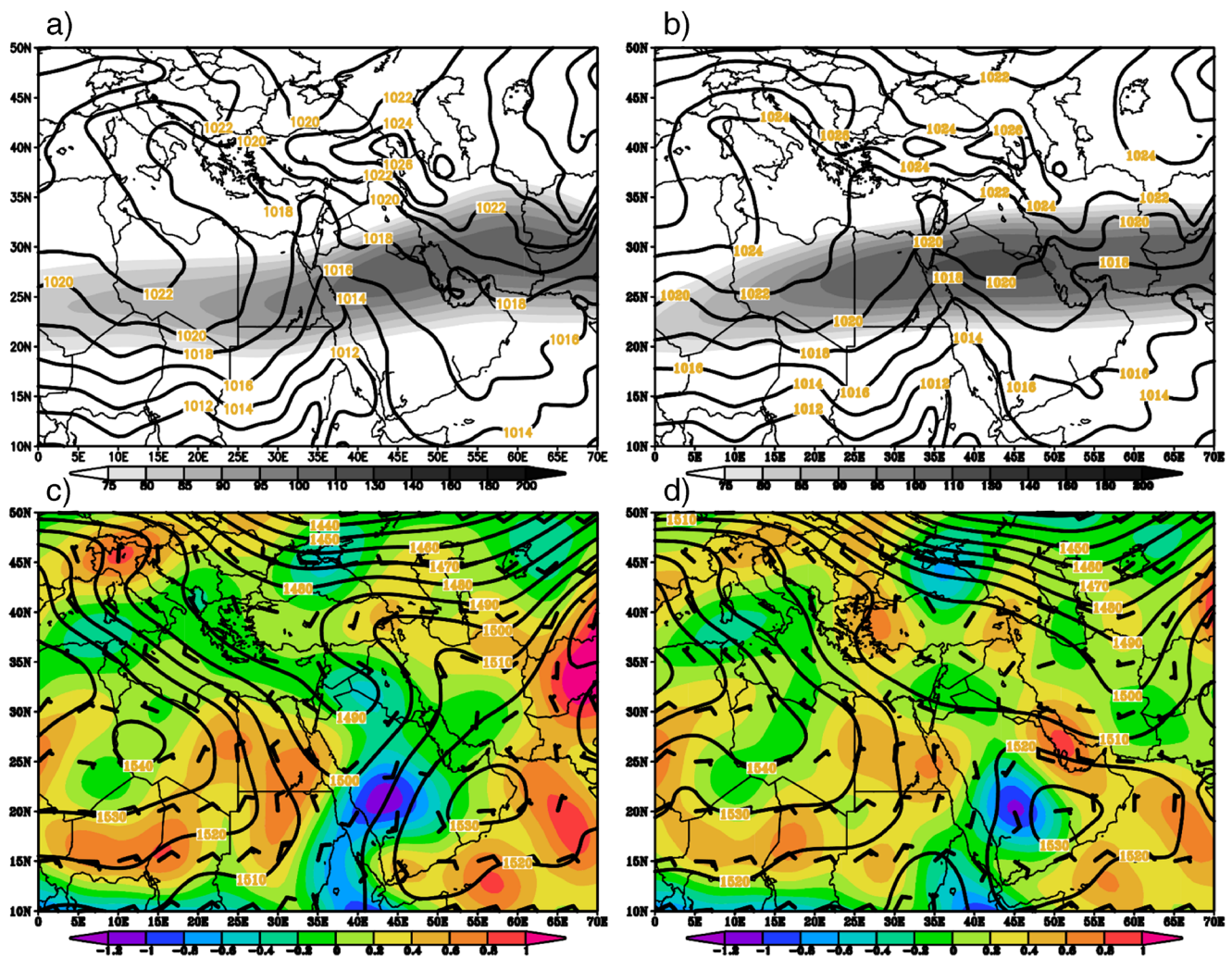


**Fig. 9** Maps of the SLP (isobars, in hPa) and maximum wind at 200 hPa (shading, in knots) for 250 hPa in January for a rainfall and b nonrainfall composites. Maps of the geopotential height (contours, in gpm), wind

(barbs, in knots) and temperature (shading, in °C) at 850 hPa for 250 hPa in January for c rainfall and d nonrainfall composites

motion form a vertical motion gradient area over the Red Sea and southeastern Mediterranean.

In the nonrainfall composite (Fig. 9d), the northern cyclone, with a value of 1430 gpm, has two troughs: a wide weak trough located over the Levant and the northern AP and a deep trough located over Pakistan and India. Additionally, two branches of the subtropical anticyclone appear: the western branch, with a value of 1560 gpm, has a pronounced ridge over the Mediterranean and Africa, while the eastern branch, with a value of 1530 gpm, is over the southern AP and has a ridge over the central AP. Additionally, the tropical cyclone, with a value of 1520 gpm, extends over the southwestern Red Sea. The wind speed weakens around the Red Sea and strengthens in the surrounding areas.

Different from the upward motion in the rainfall composite, the areas of upward motion in the nonrainfall composite (Fig. 9d) are separated in different regions,

including over the southwestern AP, with a value of  $-1.0$  Pa/s; over the central Mediterranean, with a value of  $-0.2$  Pa/s; and over the Black Sea, with a value of  $-0.6$  Pa/s. Three areas of downward motion surround the areas of upward motion: over Egypt and the Red Sea, with a value of  $0.6$  Pa/s; over the eastern AP and Arabian Gulf, with a value of  $0.8$  Pa/s; and over the northeastern Mediterranean, with a value of  $0.6$  Pa/s. These areas of upward and downward motion form a vertical motion gradient area over the southern Red Sea and eastern AP.

#### Geopotential height at 500 hPa and static stability in the 1000–500 hPa layer

In the rainfall composite (Fig. 10a), the northern cyclone, with a value of 5420 gpm, has a deep trough over the EM, northern Red Sea, and Levant, which is similar to the wet RST over the EM region (Tsvieli and Zangvil 2005). The subtropical



anticyclone, with a value of 5840 gpm, has two ridges over Africa and the mid-Mediterranean and over the Arabian Gulf. The wind speed has a high value of 55 knots over the mid-AP and decreases northward and southward.

The area of low stability over the Mediterranean, with a value of  $0.8^{\circ} \text{ db}^{-1}$ , extends over northern Africa, the Levant, and the western AP (Fig. 10a). However, the weak stability area, with a value of  $1.0^{\circ} \text{ db}^{-1}$ , over the Caspian Sea extends into a small area over northern Iran. The high-stability areas over Africa, over the northern study region, and over the Arabian Sea, with a value of  $1.2^{\circ} \text{ db}^{-1}$ , surround the low-stability area and form stability gradient areas around the Mediterranean and Red Seas.

In the nonrainfall composite (Fig. 10b), the northern cyclone, with a value of 5400 gpm, has two troughs over Iran and over the western Mediterranean. The subtropical anticyclone, with a value of 5860 gpm, has a ridge over the Red Sea.

This situation is similar to that of polar dry days over the southeastern Mediterranean (Saaroni et al. 2019), in which the negative phase of the third mode (Dunkeloh and Jacobeit 2003) produces dryness over the Levant and a dry RST over the EM region (Tsvieli and Zangvil 2005). The wind speed at this level reaches 55 knots over the mid-AP and decreases northward and southward, with a high rate of decrease southward.

The low-stability lines over the Mediterranean (Fig. 10b) are oriented over the Levant from west to east, rather than from northwest to southeast, in the rainfall composite. Additionally, a new low-stability area over the eastern study region, with a value of  $0.9^{\circ} \text{ db}^{-1}$ , extends to Iran and the Caspian Sea. The core of the high-stability area over Africa extends eastward, while the high-stability area over the Arabian Sea extends northward. These high- and low-stability areas form a relatively weak stability gradient

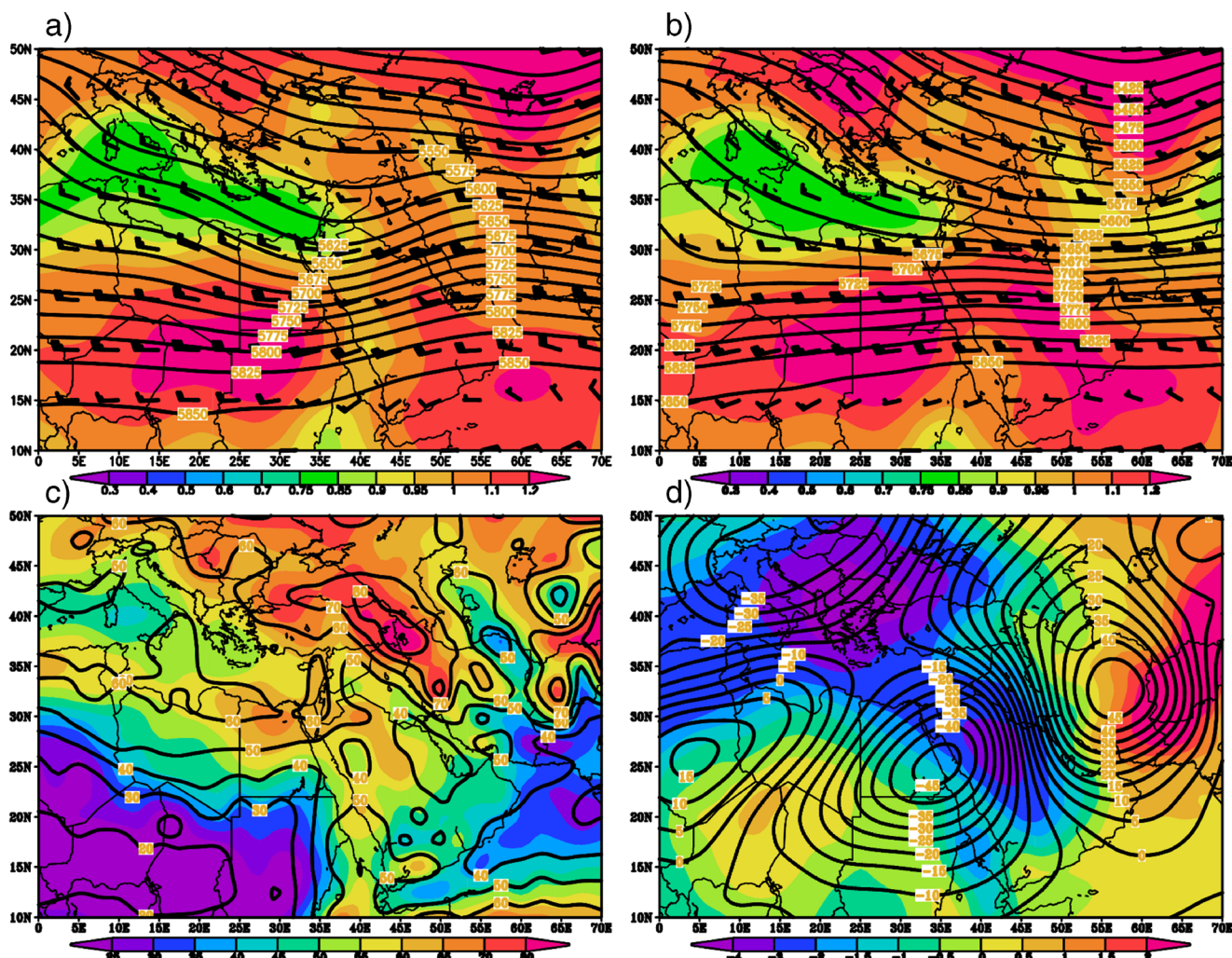


Fig. 10 Maps of the geopotential height (contours, in gpm), wind (barbs, in knots), and temperature (shading, in  $^{\circ}\text{C}$ ) at 500 hPa for 250 hPa in January for **a** rainfall and **b** nonrainfall composites. Maps of **c** the relative humidity in % (contours for nonrainfall and shading for rainfall) at

700 hPa and **d** the difference in the SLP (shading, in hPa) between rainfall and nonrainfall composites and 500 hPa geopotential height (contours in gpm) for the 250 hPa-January composites

over the Red Sea and the Levant and a relatively high stability gradient around the Mediterranean.

The vertical variation in the jet show that the rainy RST is located to the east and has an area with a relatively high gradient over the eastern Red Sea compared with that in the nonrainfall composite. Additionally, the STJ forms a trough shape over the Red Sea, while it forms a ridge shape in the nonrainfall composite.

### Relative humidity at 700 hPa and SLP/500 hPa geopotential differences

In the rainfall composite (Fig. 10c), the northwestern area of the AP has an RH greater than 60%, and the northeast area of the AP has an RH greater than 50%. Moreover, most of the Red Sea area has an RH value greater than 50%.

In the nonrainfall composite (Fig. 10c), the northwestern area of the AP has an RH greater than 50%, while the northeastern area has an RH greater than 40%. Additionally, the northern Red Sea has an RH of approximately 40%, and its southern area has an RH greater than 50%. Generally, the rainfall composite has an RH that is 10% higher than that of the nonrainfall composite.

Two maximum SLP negative difference cores (Fig. 10d) are located over the AP and southeastern Europe, with values of  $-3.5$  hPa and  $-4.5$  hPa, respectively. One maximum positive difference, with a value of 4 hPa, is located over Afghanistan. The negative difference lines are oriented northwest to southeast over the western AP and the Levant.

At 500 hPa, the highest geopotential negative difference (Fig. 10d) is located over southern Egypt and the adjacent Red Sea, with a value of  $-45$  gpm. Two positive differences are located over Africa, with a value of 15 gpm, and over the eastern region, with a value of 45 gpm, over Iran.

This distribution forms a geopotential difference oriented northeast to southwest on the western side of the maximum negative area and north to south over the eastern side of the AP. The maximum negative difference over Egypt is located to the west of the SLP difference.

## Conclusion

This study presented the synoptic features of winter rain associated with STJ variability over the northern AP. An objective method was used to specify the STJ at pressure levels between 400 and 200 hPa.

The specified STJ and the surface observations of rainfall over the northern AP indicated that most of the rainfall and the STJ in winter were found in the area between  $25^{\circ}\text{N}$  and  $30^{\circ}\text{N}$ , while the STJ was located above 200 hPa.

The study indicated that in the rainfall composite, the RST extended northward and deeply interacted with the upper

trough, the low-pressure system over the area was deepened, and the Azores and Siberian highs intensified and weakened, respectively. In contrast, the rain decreased when the lines of surface low pressure were oriented farther than the north-south direction, and the surrounding pressure gradient decreased. Furthermore, the rain decreased when the relative position of the negative difference core over the area shifted southward from the northern Red Sea.

Additionally, the upper atmospheric system indicated that the rainfall composite had a deep northern cyclone trough, with a geopotential gradient over the northern AP and EM, which was considered a factor that increased the area destabilization or a main synoptic factor for Mediterranean rain (Kutiel et al. 1996; Xoplaki et al. 2000; Dunkeloh and Jacobeit 2003).

In contrast, in the nonrainfall composite, the AP anticyclone prevented the northern cyclone trough from extending southward or forcing the trough to form a flat shape over the AP; i.e. stabilization increased over the area. Maheras et al. (2000) and Dunkeloh and Jacobeit (2003) noted that this situation decreased the cyclone frequency or was less likely to maintain the surface low-pressure system for a long period (Shay-El and Alpert 1991; Stein and Alpert 1991).

On the other hand, although December appeared to be the driest winter month, our composite cases for December showed that the northern AP was influenced by a short period of rainfall cases, and most of the cases appeared to be advected from the Mediterranean or from the region between the Caspian and Black Seas. Moreover, a difference in the SLP and 500 hPa geopotential height over the Middle East appeared small in December, which could be explained by the fact that the rainy systems in December were small-scale and intensive systems; therefore, they were smoothed out in the composite maps. Furthermore, the high negative difference over Europe may indicate that the rainy systems over the northern AP formed from the advection of Mediterranean systems.

The distinctness of the rainy composite for December compared to composites for January and February was observed by Kutiel and Paz (1998) for rainfall in the southern Levant, which may be partially attributed either to the spottiness of the rain at the beginning of the winter rainy season or to the strong relationship of the rain with upper layer systems (Ghasemi and Khalili 2008).

The results of the study demonstrated that many atmospheric systems, ranging from small to large scales, produced rainy systems in the study area, but more research is needed for full understanding. In the future, we are planning to conduct more studies considering the effectiveness of the phenomena scales and vertical changes in the jet stream streaks (i.e., three-dimensional study of the jet stream) for generating rain systems.

## References

- Abish B, Joseph PV, Ola MJ (2015) Climate change in the subtropical jet stream during 1950–2009. *Adv Atmos Sci* 32:140. <https://doi.org/10.1007/s00376-014-4156-6>
- Alpert P, Neeman BU, Shay-El Y (1990) Climatological Analysis of Mediterranean Cyclones Using ECMWF Data. *Tellus* 42:65–77
- Alpert P, Ben-Gai T, Baharad A, Benjamini Y, Yekutieli D, Colacino M, Diodato L, Ramis C, Homar V, Romero R, Michaelides S, Manes A (2002) The paradoxical increase of Mediterranean extreme daily rainfall in spite of decrease in total values. *Geophys Res Lett* 29(11):1536. <https://doi.org/10.1029/2001GL013554>
- Alpert P, Osetinsky I, Ziv B, Shafir H (2004) Semi-objective classification for daily synoptic systems: application to the eastern Mediterranean climate change. *Int J Climatol* 24(8):1001–1011. <https://doi.org/10.1002/joc.1036>
- Archer C, Caldeira K (2008) Historical trends in the jet streams. *Geophys Res Lett* 35:L08803. <https://doi.org/10.1029/2008GL033614>
- Asiri AM, Almazroui M, Adel AM (2020) Synoptic features associated with the winter variability of the subtropical jet stream over Africa and the Middle East. *Meteorol Atmos Phys*:1–13. <https://doi.org/10.1007/s00703-019-00722-4>
- Barth HJ, Steinkohl F (2004) Origin of winter precipitation in the central coastal lowlands of Saudi Arabia. *J Arid Environ* 57:101–115
- Ben-Gai T, Bitan A, Manes A, Alpert P (1993) Long term change in October rainfall patterns in southern Israel. *Theor Appl Climatol* 46:209–217
- Ben-Gai T, Bitan A, Manes A, Alpert P (1994) Long term change in annual rainfall patterns in southern Israel. *Theor Appl Climatol* 49:59–67
- Ben-Gai T, Bitan A, Manes A, Alpert P, Rubin S (1998) Spatial and temporal changes in rainfall frequency distribution patterns in Israel. *Theor Appl Climatol* 61:177–190
- Blackwell KG (2000) Tropical plumes in a barotropic model: a product of Rossby wave generation in the tropical upper troposphere. *Mon Weather Rev* 128:2288–2302
- Chakraborty A, Behera SK, Mujumdar M, Ohba R, Yamagata T (2006) Diagnosis of tropospheric moisture over Saudi Arabia and influences of IOD and ENSO. *Mon Weather Rev* 134:598–617
- Cullen HM, Kaplan A, Arkin PA, Demenocal P (2002) Impact of the North Atlantic Oscillation on Middle Eastern climate and streamflow. *Clim Chang* 55:315–338
- Dayan U, Sharon D (1980) Meteorological parameters for discriminating between widespread and spotty storms in the Negev. *Isr J Earth Sciences* 29(4):253–256
- Dayan U, Abramski R (1983) Heavy rain in the Middle East related to unusual jet stream properties. *Bull Amer Meteor Soc* 64:1138–1140
- Dayan U, Ziv B, Margalit A, Morin E, Sharon D (2001) A severe autumn storm over the Middle-East: Synoptic and mesoscale convection analysis. *Theor Appl Climatol* 69(1–2):103–122. <https://doi.org/10.1007/s007040170038>
- De Vries AJ, Tyrlis E, Edry D, Krichak SO, Steil B, Lelieveld J (2013) Extreme precipitation events in the Middle East: dynamics of the active Red Sea trough. *J Geophys Res Atmos* 118:7087–7108. <https://doi.org/10.1002/jgrd.50569>
- De Vries AJ, Feldstein SB, Riemer M, Tyrlis E, Sprenger M, Baumgart M, Fnais M, Lelieveld J (2016) Dynamics of tropical–extratropical interactions and extreme precipitation events in Saudi Arabia in autumn, winter and spring. *Q J R Meteorol Soc* 142:1862–1880
- Dunkeloh A, Jacobeit J (2003) Circulation dynamics of Mediterranean precipitation variability 1948–98. *Int J Climatol* 23(15):1843–1866
- Eshel G, Farrell BF (2000) Mechanisms of eastern Mediterranean rainfall variability. *J Atmos Sci* 57(19):3219–3232
- Evans JP, Smith RB (2006) Water vapor transport and the production of precipitation in the eastern Fertile Crescent. *J Hydrometeorol* 7:1295–1307
- Evans JP, Smith RB, Oglesby RJ (2004) Middle East climate simulation and dominant precipitation processes. *Int J Climatol* 24:1671–1694
- Flocas AA, Giles BD (1991) Distribution and intensity of frontal rainfall over Greece. *Int J Climatol* 11:429–442
- Gates WL (1961) Static stability in the atmosphere. *J. Meteor.* 18:526–533
- Ghasemi AR, Khalili D (2008) The association between regional and global atmospheric patterns and winter precipitation in Iran. *Atmos Res* 88:116–133
- Haggag M, El-Badry H (2013) Mesoscale numerical study of quasi-stationary convective system over Jeddah in November 2009. *Atmos Clim Sci* 3(1):73–86. <https://doi.org/10.4236/acs.2013.31010>
- Hasanean H, Almazroui M (2015) Rainfall: features and variations over Saudi Arabia, a review. *Climate* 3:578–626
- Iqbal MJ, Hameed S, Khan F (2013) Influence of Azores high pressure on middle eastern rainfall. *Theor Appl Climatol* 111(1–2):211–221
- Kahana R, Ziv B, Enzel Y, Dayan U (2002) Synoptic climatology of major floods in the Negev desert, Israel. *Int J Climatol* 22(7):867–882. <https://doi.org/10.1002/joc.766>
- Kalnay E, Kanamitsu M, Kistler R, Collins W, Deaven D, Gandin L, Iridell M, Saha S, White G, Woollen J, Zhu Y, Chelliah M, Ebisuzaki W, Higgins W, Janowiak J, Mo KC, Ropolewski C, Wang J, Leetma A, Reynolds R, Jenne R, Joseph D (1996) The NCEP/NCAR 40-year Reanalysis project. *Bull Am Meteorol Soc* 77: 437–471.
- Kelley CP, Mohtadi S, Cane MA, Seager R, Kushnir Y (2015) Climate change in the fertile crescent and implications of the recent Syrian drought. *Proceedings of National Academy of Sciences of the United States of America* 112(11):3241–3246
- Kiladis GN, Weickmann KM (1992) Circulation anomalies associated with tropical convection during northern winter. *Mon Weather Rev* 120:1900–1923
- Kistler R, Collins W, Saha S, White G, Woollen J, Kalnay E, Chelliah M, Ebisuzaki W, Kanamitsu M, Kousky V, van den Dool H, Jenne R, Fiorino M (2001) The NCEP/NCAR 50-year reanalyses: monthly CD-ROM and documentation. *Bull Am Meteorol Soc* 82:247–267
- Knippertz P (2005) Tropical–extratropical interactions associated with an Atlantic tropical plume and subtropical jet streak. *Mon Weather Rev* 133:2759–2776
- Kobrossi J, Karam F, Mitri G (2021) Rain pattern analysis using the Standardized Precipitation Index for long-term drought characterization in Lebanon. *Arab J Geosci* 14:44. <https://doi.org/10.1007/s12517-020-06387-3>
- Koch P, Wernli H, Davies HC (2006) An event-based jet-stream climatology and typology. *Int J Climatol* 26:283–301
- Krichak SO, Tsidulko M, Alpert P (2000) Monthly synoptic patterns with wet/dry conditions in the eastern Mediterranean. *Theor Appl Climatol* 65:215–229
- Krishnamurti T (1961) The subtropical jet stream of winter. *18 Journal of Meteorology*
- Kutieli H (1991) Recent spatial and temporal variations in mean sea level pressure over Europe and the Middle East, and their influence on the rainfall regime in the Galilee. *Theor Appl Climatol* 44:151–166
- Kutieli H, Paz S (1998) Sea level pressure departures in the Mediterranean and their relationship with monthly rainfall conditions in Israel. *Theor Appl Climatol* 60:93–109
- Kutieli H, Maheras P, Guika S (1996) Circulation and extreme rainfall conditions in the eastern Mediterranean during the last century. *Int J Climatol* 16:73–92
- Lockwood JG (1988) Climate and climatic variability in semi-arid regions at low latitudes. In *The Impact of Climatic Variations on Agriculture, Vol. 2: Assessments in Semi-Arid Regions*, Porry ML, et al., (eds); 85–120

- Maheras P, Patrikas I, Karacostas Th, Chr Anagnostopoulou (2000) Automatic classification of circulation types in Greece: methodology, description, frequency, variability and trend analysis. *Theor Appl Climatol* 67:205–223
- Maheras P, Flocas HA, Patrikas I, Chr Anagnostopoulou (2001) A 40 year objective climatology of surface cyclones in the Mediterranean region: spatial and temporal distribution. *Int J Climatol* 21(1):109–130. <https://doi.org/10.1002/joc.599>
- Martius O, Sodemann H, Joos H, Pfahl S, Winschall A, Croci-Maspoli M, Graf M, Madonna E, Mueller B, Schemm S, Sedlacek J, Sprenger M, Wernli H (2013) The role of upper-level dynamics and surface processes for the Pakistan flood of July 2010. *Q J R Meteorol Soc* 139:1780–1797
- Mashat A, Basset HA (2011) Analysis of Rainfall over Saudi Arabia. *JKAU: Met. Env Arid Land Agric Sci* 22:59–78. <https://doi.org/10.4197/Met.22-2.4>
- Niranjan Kumar K, Ouarda TBMJ, Sandeep S, Ajayamohan RS (2016) Wintertime precipitation variability over the Arabian Peninsula and its relationship with ENSO in the CAM4 simulations. *Clim Dyn* 47: 1–12. <https://doi.org/10.1007/s00382-016-2973-2>
- Oikonomou C, Flocas HA, Hatzaki M, Nisantzi A, Asimakopoulos DN (2010) Relationship of extreme dry spells in eastern Mediterranean with large-scale circulation. *Theor Appl Climatol* 100(1–2):137–151
- Parolari AJ, Li D, Bou-Zeid E, Katul GG, Assouline S (2016) Climate, not conflict, explains extreme Middle East dust storm. *Environ Res Lett* 11:114013
- Qaisrani ZN, Nuthammachot N, Techato K et al (2021) Drought monitoring based on standardized precipitation index and standardized precipitation evapotranspiration Index in the arid zone of Balochistan province, Pakistan. *Arab J Geosci* 14:11. <https://doi.org/10.1007/s12517-020-06302-w>
- Raymond F, Ullmann A, Camberlin P, Oueslati B, Drobinski P (2018) Atmospheric conditions and weather regimes associated with extreme winter dry spells over the Mediterranean basin. *Clim Dyn* 50:4437–4453. <https://doi.org/10.1007/s00382-017-3884-6>
- Raziei T, Arasteh PD, Saghafian B (2005) Annual rainfall trend in arid and semi arid region of Iran. ICID21st European Regional Conference, pp. 1–8
- Rogers JC (1990) Patterns of low-frequency monthly sea level pressure variability (1899–1986) and associated wave cyclone frequencies. *J Clim* 3:1364–1379
- Saaroni H, Ziv B, Harpaz T, Lempert J (2019) Dry events in the winter in Israel and its linkage to synoptic and large-scale circulations. *Int J Climatol* 39:1054–1071. <https://doi.org/10.1002/joc.5862>
- Seager R, Harnik N, Kushnir Y, Robinson W, Miller J (2003) Mechanisms of hemispherically symmetric climate variability. *J Clim* 16:1960–1978
- Shay-El Y, Alpert P (1991) A diagnostic study of winter diabatic heating in the Mediterranean in relation with cyclones. *Q J Roy Meteor Soc* 117:715–747
- Stein U, Alpert P (1991) Inclusion of sea moisture flux in the Anthes-Kuo cumulus parametrization. *Contr Atmos Phys* 64:231–243
- Steinberger EH, Gazit-Yaari N (1996) Recent changes in spatial distribution of annual precipitation in Israel. *J Clim* 9:3328–3336
- Strong C, Davis RE (2005) The surface of maximum wind as an alternative to the isobaric surface for wind climatology. *Geophys Res Lett* 32:L04813. <https://doi.org/10.1029/2004GL022039>
- Strong C, Davis RE (2007) Winter jet stream trends over the Northern Hemisphere. *Quart J Roy Meteor Soc* 133:2109–2115
- Tramblay Y, Hertig E (2018) Modelling extreme dry spells in the Mediterranean region in connection with atmospheric circulation. *Atmos Res* 202:40–48
- Trewartha GT, Horn LH (1980) *Introduction to Climate*, 5th edn. McGraw Hill, New York, NY
- Trigo IF, Davies TD, Bigg GR (1999) Objective climatology of cyclones in the Mediterranean region. *J Climate* 12(6):1685–1696
- Tsvieli Y, Zangvil A (2005) Synoptic climatological analysis of “wet” and “dry” Red Sea Troughs over Israel. *Int J Climatol* 25:1997–2015. <https://doi.org/10.1002/joc.1232>
- Xoplaki E, Luterbacher J, Burkard R, Patrikas I, Maheras P (2000) Connection between the large-scale 500 hPa geopotential height fields and precipitation over Greece during wintertime. *Clim Res* 14:129–146
- Ziv B (2001) A subtropical rainstorm associated with a tropical plume over Africa and the Middle-East. *Theor Appl Climatol* 68:91–102
- Ziv B, Dayan U, Sharon D (2005) A mid-winter, tropical extreme flood-producing storm in southern Israel: synoptic scale analysis. *Meteorol Atmos Phys* 88:53–63
- Ziv B, Dayan U, Kushnir Y, Roth C, Enzel Y (2006) Regional and global atmospheric patterns governing rainfall in the southern Levant. *Int J Climatol* 26:55–73
- Ziv B, Saaroni H, Pargament R, Harpaz T, Alpert P (2014) Trends in rainfall regime over Israel, 1975–2010, and their relationship to large scale variability. *Reg Environ Chang* 14(5):1751–1764. <https://doi.org/10.1007/s10113-013-0414-x>